Research Square

Preprints are preliminary reports that have not undergone peer review.
They should not be considered conclusive, used to inform clinical practice,
or referenced by the media as validated information.

Genome-Wide Identification of the Potato MAPKKKK Gene Family Reveals StMAPKKKK1 as a Positive Regulator of Salt and Drought Tolerance

Xi zhu

zhuxi@catas.cn

South Subtropical Crops Research Institute https://orcid.org/0000-0002-6563-6582

Research Article

Keywords: Potato, StMAPKKKK1, Salt and drought, Osmotic adjustment, Antioxidant defense

Posted Date: November 6th, 2026

DOI: https://doi.org/10.21203/rs.3.rs-11631012/v1

License: This work is licensed under a Creative Commons Attribution 4.0 International License.
Read Full License

Additional Declarations: The authors declare no competing interests.

Title: Genome-Wide Identification of the Potato *MAPKKKK* Gene Family Reveals *StMAPKKKK1* as a Positive Regulator of Salt and Drought Tolerance

Xiaoqin Duan [1,2,3,4], Xi Zhu [2,4*], Ning Zhang [1,3], Kaitong Wang [1,3], Zhilin Han [1,3], Yu Zhang [2,4], Yasir Majeed [1,3], Hui Jin [2,4], Xidan Pang [2], Dong Zhou [2], Zhuo Chen [2], Huaijun Si [1,3*]

dxq2755545382@163.com (X.D.); zhuxi@catas.cn (X.Z.); ningzh@gsau.edu.cn (N.Z.); kait_wang@163.com (K.W.); 13619098135@163.com (Z.H.); zhangyu@catas.cn (Y.Z.); yasirmajeed5453@gmail.com (Y.M.); jinh@catas.cn (H.J.); pangxidan@catas.cn (X.P.); 15574994586@163.com (D.Z.); chenzhuo@catas.cn (Z.C.); hjsi@gsau.edu.cn (H.S.)

[1] State Key Laboratory of Aridland Crop Science, College of Agronomy, Gansu Agricultural University, Lanzhou 730070, China

[2] Key Laboratory of Tropical Fruit Biology, Ministry of Agriculture and Rural Affairs/Key Laboratory of Postharvest Physiology and Technology of Tropical Horticultural Products of Hainan Province, South Subtropical Crops Research Institute, Chinese Academy of Tropical Agricultural Sciences, Zhanjiang, Guangdong 524091, China.

[3] College of Life Science and Technology, Gansu Agricultural University, Lanzhou 730070, China

[4] National Key Laboratory for Tropical Crop Breeding, Sanya Research Institute, Chinese Academy of Tropical Agricultural Sciences, Sanya 572025, China.

[*] Author to whom correspondence should be addressed.

Corresponding E-mail: zhuxi@catas.cn (X.Z.); hjsi@gsau.edu.cn (H.S.)

Abstract

Mitogen-activated protein kinase kinase kinase kinases (MAP4Ks/MAPKKKKs) reside at the apex of MAPK signalling cascades, yet their roles in potato abiotic stress responses remain unexplored. Here, we identified eight *StMAPKKKK* genes via genome-wide identification in potato. StMAPKKKK1 protein was strongly induced by salt and drought stress and localized to the plasma membrane and cytoplasm. Yeast two-hybrid (Y2H), bimolecular fluorescence complementation (BiFC), and split-luciferase complementation (SLC) experiments show that StMAPKKKK1 physically interacts with StMAPKK2. To assess its function, we generated *StMAPKKKK1*-overexpressing (OE) and RNA interference (RNAi) lines in potato cultivar *'Atlantic'*. OE lines exhibited improved growth, with higher plant height, biomass, and leaf number, whereas RNAi lines were more sensitive than non-transgenic (NT) controls under both salt and drought stress conditions. Higher activities of ascorbate peroxidase (APX), catalase (CAT), superoxide dismutase (SOD), and peroxidase (POD), as well as proline and total chlorophyll contents, along with lower levels of hydrogen peroxide (H_2O_2) and malondialdehyde (MDA) were observed in OE lines. In contrast, RNAi lines showed opposite trends for all above-mentioned parameters. These results indicate alleviated oxidative damage, enhanced osmotic adjustment, and better pigment retention. This study presents the first functional characterization of the *StMAPKKKK* family in potato and establishes *StMAPKKKK1* as a positive regulator of salt and

drought tolerance, acting at least partially through interaction with StMAPKK2 and activation of the antioxidant defense system.

Keywords: Potato; *StMAPKKKK1*; Salt and drought; Osmotic adjustment; Antioxidant defense.

1. Introduction

Globally, potato (Solanum tuberosum L.) is the fourth most important staple food crop, surpassed only by maize, wheat, and rice, and supplies substantial amounts of carbohydrates, vitamins, minerals, and dietary fiber to a large share of the global population (Zaheer and Akhtar, 2016; Li et al., 2024a). Its high-yielding potential, broad adaptability, and nutritional value make it indispensable for global food and nutritional security, particularly under increasing population pressure and changing climatic conditions (Bravo Iniguez et al., 2026). Vegetative growth and yield in potato are severely constrained by drought and salinity, two of the most prevalent abiotic stresses. Owing to its high water requirement and sensitivity to water and salt stress, potato experiences impaired water uptake, disrupted ion homeostasis, reduced photosynthetic activity, and restricted vegetative and stolon growth under these conditions (Levy et al., 2013; Bai et al., 2016; George et al., 2017). Moreover, these stresses induce oxidative and osmotic stress, leading to loss of membrane integrity, over-accumulation of reactive oxygen species (ROS), and metabolic disruption, which ultimately constrain tuber development and reduce both yield and quality (Bai et al., 2016; Wen et al., 2025; Zhang et al., 2025). Recent evidence further shows that drought and salt stress reduce photosynthetic performance and disrupt leaf microstructure, while simultaneously enhancing ROS accumulation and antioxidant responses, with combined stress causing more pronounced effects (Zhang et al., 2025). Potatoes have evolved sophisticated adaptive mechanisms to restore cellular homeostasis, involving calcium signaling, phytohormones, antioxidant defense systems, transcriptional regulation, and mitogen-activated protein kinase (MAPK) signaling. However, the upstream molecular regulators orchestrating these interconnected responses remain incompletely understood (Xu and Zhang, 2015; Kaufmann et al., 2010; He et al., 2018; Komis et al., 2018; Waadt et al., 2022). Therefore, identifying key upstream signaling components that coordinate stress perception and downstream defense responses is essential for accelerating the development of climate-resilient potato cultivars through molecular breeding and genetic engineering.

Among the signaling pathways regulating plant adaptation to environmental stresses, the MAPK cascade is one of the most highly conserved phosphorylation signaling modules, controlling plant growth, development, hormone signaling, immunity, and abiotic stress responses (Komis et al., 2018; Zhang and Zhang, 2022). In plants, MAPK signaling is organized as a hierarchical phosphorylation cascade comprising four sequential kinase tiers: MAPK kinase kinase kinases (MAPKKKKs/MAP4Ks), MAPK kinase kinases (MAPKKKs), MAPK kinases (MAPKKs), and MAPKs. As the uppermost regulatory components, MAP4Ks initiate signal transduction by phosphorylating and modulating specific MAPKKKs through protein–protein interactions, thereby linking upstream stress perception to downstream MAPK signaling. Activated MAPKKKs, which are classified into the MEKK, Raf, and ZIK subfamilies, subsequently phosphorylate conserved serine/threonine residues within the S/T-$X_{3–5}$-S/T activation motif of MAPKKs. These phosphorylation events trigger MAPK activation through the dual phosphorylation of the highly conserved threonine (Thr) and tyrosine (Tyr) residues within the

TXY motif of the activation loop (TEY or TDY) (Jonak et al., 2002; Champion et al., 2004; Rodriguez et al., 2010; Manna et al., 2023). Activated MAPKs ultimately phosphorylate numerous downstream substrates, including transcription factors, metabolic enzymes, and regulatory proteins in both the cytoplasm and nucleus, thereby reprogramming gene expression and cellular metabolism to coordinate physiological adaptation to environmental stresses (Pedley and Martin, 2005; Komis et al., 2018; Zhang & Zhang, 2022). While MAPKKKs function as central signaling hubs integrating diverse upstream signals (Ichimura et al., 2002; Colcombet and Hirt, 2008), accumulating evidence demonstrates that many plant MAPK pathways are initiated by an additional upstream kinase layer, MAPKKKKs (MAP4Ks), revealing a previously underappreciated level of regulatory complexity. This additional kinase tier enhances signaling specificity and amplification, highlighting MAP4Ks as critical upstream regulators that coordinate extracellular signal perception with intracellular MAPK-mediated stress responses (Jonak et al., 2002).

Unlike canonical MAPKKKs, MAP4Ks belong predominantly to the Ste20 kinase superfamily and possess a highly conserved serine/threonine kinase domain containing the characteristic T/S-X_5-T/S phosphorylation motif between kinase subdomains VII and VIII, which is essential for catalytic activity and substrate recognition (Jouannic et al., 1999; Ichimura et al., 2002). Plant MAP4Ks display diverse domain architectures, enabling interactions with receptor-like kinases, membrane lipids, adaptor proteins, and small GTPases, thereby functioning as molecular bridges between extracellular signal perception and intracellular MAPK phosphorylation cascades (Jouannic et al., 1999; Pan et al., 2021; Li et al., 2024b). In addition to activating downstream MEKK- and Raf-type MAPKKKs, MAP4Ks can function as scaffold proteins that enhance signaling specificity, amplification, and pathway fidelity, allowing the precise integration of developmental, hormonal, and environmental signals (Dan et al., 2001; Taj et al., 2010). Genome-wide analyses indicate that the MAP4K family is evolutionarily conserved across higher plants but has undergone lineage-specific expansion during genome evolution, with 10 members identified in *Arabidopsis thaliana* (Ichimura et al., 2002; Champion et al., 2004), 7 in rice (*Oryza sativa*) (Pan et al., 2021), 11 in maize (*Zea mays*) (He et al., 2026), and 25 in hexaploid wheat (*Triticum aestivum*) (Li et al., 2024b). Functional characterization of plant MAP4Ks demonstrates that they participate in multiple biological processes, particularly abiotic stress adaptation. Under salt stress, rice *OsMAPKKKK6* positively regulates salinity tolerance by directly phosphorylating *OsMKK6* at Ser13, thereby maintaining Na^+/K^+ homeostasis (Ren et al., 2026). Likewise, cotton *GhMAPKKKK13* enhances both salt and drought tolerance, as demonstrated by improved stress resistance in transgenic plants and increased susceptibility following gene silencing (Zeng et al., 2025). During drought stress and ABA signaling, Arabidopsis *MAPKKKK1* and *MAPKKKK2* function downstream of *OST1* and contribute to the regulation of ABA-induced stomatal closure and drought tolerance, thereby promoting plant adaptation to water deficit (Tang et al., 2025; Hu et al., 2026). In wheat, a putative *MAPKKKK10–MEKK7–MKK11–MAPK6* signaling cascade has also been proposed to contribute to drought tolerance (Li et al., 2024b). In pepper, *CaMAP4K3* functions as a negative regulator of drought resistance (Lim et al., 2025). Beyond abiotic stress, MAP4Ks are also involved in developmental and environmental signaling. In *Arabidopsis*, *MAPKKKK3* (*SIK1*) regulates cell proliferation and expansion, whereas *MAPKKKK10* (BLUS1) functions downstream of phototropins to promote blue-light-induced stomatal opening.

Specifically, phototropins phosphorylate BLUS1, representing an early step in the signaling pathway that activates stomatal opening (Takemiya et al., 2013; Xiong et al., 2016). Similarly, in *Arabidopsis*, *AtMAPKKKK4* (*SIK1*) contributes to membrane-associated immune signaling through its interaction with the receptor-like cytoplasmic kinase *BIK1* (Jiang et al., 2019). MAP4Ks can establish direct protein–protein interactions with diverse signaling components, enabling their integration into distinct cellular pathways. For example, *Arabidopsis* SIK1 directly interacts with and phosphorylates *BIK1* during immune signaling, while *MAP4K1/2* interact with and are phosphorylated by *OST1* in ABA- and drought-related signaling (Zhang et al., 2018; Tang et al., 2025; Hu et al., 2026).

In potato, considerable progress has been made in elucidating the roles of components of the canonical MAPK cascade in abiotic stress responses. Genome-wide studies have identified and characterized the *StMAPK*, *StMAPKK*, and *StMAPKKK* gene families, providing insights into their evolutionary relationships, structural characteristics, and stress-responsive expression patterns (Shang et al., 2022; Zhu et al., 2026). Functional analyses have demonstrated that several StMAPKs, including *StMAPK1/3/7/10/11/19,* positively regulate potato adaptation to drought, salinity, cold, and heat stresses through modulation of stress-responsive signaling pathways (Zhu et al., 2020, 2021, 2023, 2025a, 2025b; Majeed et al., 2024; Luo et al., 2025). Likewise, *StMAPKK1/5* have been functionally characterized and shown to participate in drought, salt, and heat stress responses (Luo et al., 2024; Zhu et al., 2024, 2025c; Wang et al., 2025). A subsequent investigation documented that *StMAPKKK44* functions as a positive modulator of both drought and salinity tolerance in potato, thereby reinforcing the essential contribution of the conventional MAPK signaling module to stress acclimation (Zhu et al., 2026). Despite these advances, the upstream MAP4K layer remains completely unexplored in potato. To date, a systematic examination of the *StMAPKKKK* gene family in potato has yet to be conducted, and whether potato MAP4Ks participate in conferring resistance to salt and drought remains experimentally unconfirmed. Consequently, the identification, evolutionary characteristics, tissue-specific expression divergence patterns, and the biological functions of the *StMAPKKKK* gene family in mediating potato responses to salt and drought stress remain elusive. To bridge these knowledge gaps, we performed a systematic characterization of the *StMAPKKKK* gene family in potato, covering phylogenetic relationships, cis-regulatory elements within the promoter regions, tissue-specific expression profiles, and stress-responsive transcriptional dynamics. Through subcellular localization, protein–protein interaction assays, and physiological analyses under salinity and drought stress conditions, we characterized the function of *StMAPKKKK1* and identified it as a potential candidate for enhancing crop stress tolerance through molecular breeding.

2. Materials and Methods

2.1.Bioinformatics analysis

2.1.1. Identification of StMAPKKKK genes

To comprehensively identify members of the potato MAPKKKK (MAP4K) gene family, the genome assemblies and annotation files of *Solanum tuberosum* v6.1 (doubled-monoploid DM1-3 516 R44; Pham et al., 2020), Oryza sativa v7.0 (Ouyang et al., 2007) and Arabidopsis thaliana TAIR10 (Lamesch et al., 2012) were retrieved from Phytozome v14 (Goodstein et al.,

2012; https://phytozome.jgi.doe.gov), and the deduced proteomes were extracted. A local potato protein database was constructed with makeblastdb from the BLAST+ package (Camacho et al., 2009). The previously reported AtMAPKKKK (Jonak et al., 2002) and OsMAPKKKK (Ren et al., 2026) protein sequences were used as queries in BLASTP searches against this database (E-value ≤ 1e-5), and the resulting hits were further filtered to retain candidates with ≥ 50% sequence identity and ≥ 50% query coverage. In parallel, the query sequences were aligned with MUSCLE (Edgar, 2004), and a family-specific hidden Markov model (HMM) profile was built from the resulting alignment using hmmbuild in HMMER 3.4 (Eddy, 2011; http://hmmer.org); the profile was searched against the potato proteome with hmmsearch (E-value ≤ 1e-5). The candidates recovered by both strategies were merged, and conserved domains were annotated with PfamScan against the Pfam-A database (version 35.0; Mistry et al., 2021) using the Pfam gathering thresholds (--cut_ga); sequences lacking the protein kinase domain (PF00069) or carrying a truncated PF00069 domain (coverage < 70%) were discarded. Redundancy was then removed by collapsing identical sequences and retaining only the longest transcript per gene locus as the representative isoform, ultimately yielding 8 non-redundant *StMAPKKKK* genes. For each *StMAPKKKK* gene, the genomic sequence length, chromosomal start and end coordinates, and coding sequence (CDS) length were retrieved from Phytozome v14. The ExPASy ProtParam tool (default parameters; Gasteiger et al., 2005; https://web.expasy.org/protparam/) was employed to compute the physicochemical properties of the predicted StMAPKKKK proteins, namely molecular weight, theoretical isoelectric point (pI), instability index, aliphatic index, and grand average of hydropathicity (GRAVY). These properties, together with the corresponding gene accession numbers, chromosomal positions, and protein lengths, are provided in Table S1.

2.1.2. Chromosomal mapping, duplication patterns, and evolutionary relationships

The physical positions of the identified *StMAPKKKK* loci on potato chromosomes were determined from the *Solanum tuberosum* v6.1 genome annotation in Phytozome v14 (Goodstein et al., 2012; Pham et al., 2020), and the chromosomal distribution was drawn with MapGene2Chrom (MG2C v2.0; Chao et al., 2021; http://mg2c.iask.in/mg2c_v2.0/) based on the physical coordinates. For intra-genomic duplication analysis, an all-vs-all BLASTP search was performed against the potato proteome (-outfmt 6; E-value cutoff 1e-10; top five hits retained). The resulting hit table, together with the gene position (BED) file, was used to detect collinear blocks with MCScanX (Wang et al., 2012) under default parameters, and duplication modes were further classified using the duplicate_gene_classifier program. The intra-genomic collinear blocks were visualized as a Circos plot (Krzywinski et al., 2009) in TBtools v2.0 (Chen et al., 2023). For each pair of duplicated *StMAPKKKK* genes located within collinear blocks, the numbers of nonsynonymous (Ka) and synonymous (Ks) substitutions per site and their ratio (Ka/Ks) were estimated with TBtools (version 2.0; Chen et al., 2023) using the Nei–Gojobori (NG86) method (Nei and Gojobori, 1986), based on codon alignments generated from the corresponding protein alignments; gene pairs with Ks > 2.0 were excluded to avoid substitution saturation. For phylogenetic reconstruction, MAPKKKK protein sequences of *Arabidopsis thaliana* (TAIR10) and *Oryza sativa* (v7.0) were retrieved from Phytozome v14 and combined with the 8 potato StMAPKKKK sequences identified in this study. The combined dataset was aligned with MUSCLE (Edgar, 2004), and a neighbor-joining tree (Saitou and Nei, 1987) was reconstructed in MEGA 11 (Tamura et al., 2021) under the Poisson correction model with pairwise deletion of gaps

and missing data; branch support was assessed with 1,000 bootstrap replicates, and clades with bootstrap support ≥ 50% are indicated on the tree. For inter-species synteny analysis, all-vs-all BLASTP alignments between potato and each of *Arabidopsis* and rice were performed using BLAST+ v2.12 (Camacho et al., 2009; E-value ≤ 1e-10; top five hits retained), and syntenic blocks were identified with MCScanX (Wang et al., 2012) based on the BLASTP tabular output and the corresponding gene position (BED) files. The orthologous pairs between potato and the two other species were visualized with TBtools v2.0 (Chen et al., 2023) as a three-layer chromosome comparison plot.

2.1.3. Conserved motif identification and gene structure analysis

MEME Suite (version 5.3.0; Bailey et al., 2015; http://meme-suite.org) was employed to identify conserved motifs in the StMAPKKKK proteins. The analysis allowed a maximum of 20 motifs, motif widths were constrained to 6–50 amino acid residues, and the zero-or-one-occurrence-per-sequence (ZOOPS) site-distribution model was applied, with all other parameters left at default settings. The resulting spatial distribution of the 20 motifs along each protein, together with the corresponding sequence logos, was visualized using TBtools v2.0 (Chen et al., 2023). To visualize sequence conservation between potato and *Arabidopsis* MAPKKKK proteins, full-length amino acid sequences of the StMAPKKKK and AtMAPKKKK proteins were aligned using ClustalW (Thompson et al., 1994) under default parameters. The alignment was visualized in Jalview 2.11 (Waterhouse et al., 2009) with the Zappo coloring scheme according to residue physicochemical properties. Conserved kinase motifs—including the glycine-rich motif, the invariant lysine residue, the HRD motif, the DFG motif and the MAP4K family signature motif—were manually annotated based on the Pfam PF00069 protein kinase domain profile (Mistry et al., 2021); fully conserved residues were marked with asterisks. Putative functional domains within the identified motifs were annotated using InterProScan (Jones et al., 2014; Blum et al., 2021; http://www.ebi.ac.uk/interpro/). Genomic and coding sequences of each *StMAPKKKK* locus were retrieved from the *S. tuberosum* v6.1 annotation in Phytozome v14 and submitted to GSDS 2.0 (Hu et al., 2015; http://gsds.gao-lab.org/) in FASTA format, with sequence IDs kept consistent between the two files, to generate exon-intron structure diagrams.

2.1.4. Promoter Architecture and Cis-Regulatory Element Profiling of StMAPKKKK Genes

The putative promoter region of each StMAPKKKK gene was defined as the 2-kb genomic sequence immediately upstream of the translation start codon (ATG), which was extracted with a custom Perl script. For the identification and categorization of cis-acting regulatory elements, which enabled inferences about their potential functions in modulating transcription, these putative promoter sequences were then queried against the PlantCARE database (Lescot et al., 2002; http://bioinformatics.psb.ugent.be/webtools/plantcare/html/). The distribution of the identified elements along the 2-kb promoter was visualized with TBtools v2.0 (Chen et al., 2023).

2.2.Plant materials and growth conditions

The tetraploid potato Solanum tuberosum L. cv. 'Atlantic' obtained from the Gansu Agricultural University (Lanzhou, China) served as the plant material. All transgenic and non-transgenic (NT) plants were grown *in vitro* and multiplied at the South Subtropical Crops Research Institute of the

Chinese Academy of Tropical Agricultural Science in Zhanjiang, Guangdong Province, China. Plant tissue cultures were established on Murashige and Skoog (MS) basal salt medium containing 30 g L^{-1} sucrose and 7 g L^{-1} agar. Before sterilization, the medium pH was set to 5.8–6.0, followed by autoclaving and aseptic distribution into culture vessels. The cultures were grown in a programmable MGC-450HP LED chamber (YiHeng Scientific Instruments, Shanghai, China), maintained at 21 °C with a 16-h photoperiod, an 8-h dark period, and a light intensity of 2800 lux.

2.3. Stress treatments and sampling procedures

The experimental materials included uniform 4-week-old virus-free plantlets. The apical and basal portions were excised and discarded, and the remaining stems were cut into uniform 2-cm segments, each bearing two axillary buds. Each segment was established individually in a 150-mL Erlenmeyer flask containing 30 mL of liquid MS basal medium supplemented with sucrose (30 g L^{-1}); the pH was adjusted to 5.8 ± 0.1 prior to autoclaving. At a constant temperature of 21 °C under a 16 h light and 8 h dark photoperiod (2800 lux), the cultures were sustained for a 4-week establishment period. The resulting plantlets were then transferred to freshly prepared liquid MS medium enriched with NaCl (30, 75, or 150 mM) or PEG-6000 (5%, 10%, or 20%, w/v), whereas control plantlets were transferred in parallel to fresh stress-free medium. Leaf tissue was harvested at 0, 1, 2, 4, 8, 16, 24, and 48 h after the onset of treatment. Nine independent biological replicates were used per treatment, each consisting of leaf material pooled from three plantlets. Explants (2-cm stem segments each bearing two axillary buds) were prepared as described above and pre-cultured in liquid MS medium for 2 weeks to analyze the tissue-specific expression patterns of *StMAPKKKKs*. Microtuberization was initiated by transferring the explants to a liquid MS medium without agar, containing 80 g·L^{-1} sucrose and adjusted to pH 5.8 ± 0.1. The cultures were subsequently maintained under complete darkness for 6 weeks to promote microtuber development. After natural dormancy break, 30 microtubers with approximately 1 mm sprouts were selected and transplanted into pots (24 cm diameter × 30 cm height) containing a 1:1 (v/v) mixture of nutrient soil and vermiculite. The potting substrate had a pH of 5.5–6.0, a bulk density of 0.52 g cm^{-3}, and a total porosity of 58.3%. Total organic matter, total N, total P, and total K were 12.2, 1.83, 1.57, and 16.25 g kg^{-1}, respectively, whereas available N, P, and K were 25.18, 36.76, and 146.9 mg kg^{-1}. Throughout cultivation, moisture was replenished with deionized water to maintain relative substrate water content at 70–75%, and volumetric water content was monitored at regular intervals using a TDR300 time-domain reflectometry probe from Decagon Devices, Pullman, WA, USA. Plants grown in pots were kept in a controlled growth facility at the Institute of Tropical Crops, Chinese Academy of Tropical Agricultural Sciences, Zhanjiang, Guangdong, China (21°10′ N, 110°33′ E). Fluorescent illumination was supplied at approximately 3400 lux for 16 h daily, while the temperature was maintained at 21 °C during the light period and 16 °C during darkness. Each pot received 100 mL of nutrient solution (pH 5.8) once a week, containing 1.3 mmol·L^{-1} $(NH_4)_2SO_4$, 11 mmol·L^{-1} KNO_3, 2.8 mmol·L^{-1} KH_2PO_4, 0.20 mmol·L^{-1} $FeSO_4$, 2.08 mmol·L^{-1} $MgSO_4$, 1.1 mmol·L^{-1} $CaCl_2$, 0.5 mmol·L^{-1} $MnSO_4·H_2O$ and 0.05 mmol·L^{-1} $ZnSO_4·7H_2O$. At the full flowering stage (>90% of plants at anthesis), roots, stems, leaves, and flowers were sampled from nine randomly selected plants; after natural senescence and withering of the aerial parts, tubers were collected from a further nine randomly selected plants. After collection, the plant tissues were rapidly cryopreserved in liquid nitrogen and kept at −80 °C until total RNA extraction and qRT-PCR analysis were conducted to assess the expression levels of *StMAPKKKK* genes. In parallel, two distinct stress challenge trials were implemented. The first

trial, intended for the quantification of growth-related parameters, employed uniformly grown, virus-free four-week-old transgenic and NT lines. After excising the shoot apex and basal portion through an identical cutting procedure, internodal sections each carrying two lateral buds were trimmed to a standardized length of 2 cm. These explants were subsequently immersed in liquid MS medium amended with escalating doses of either sodium chloride (30, 75, or 150 mM) or polyethylene glycol 6000 (5%, 10%, or 20% w/v) as a component of an initial screening protocol. The results showed that NaCl concentrations ≥75 mM and PEG-6000 concentrations ≥10% severely inhibited root growth, rendering the explants unable to survive during subsequent culture. Therefore, only 30 mM NaCl and 5% (w/v) PEG-6000 were adopted as the stress treatment concentrations in the formal experiment, with conventional MS liquid medium (without any stress agent) serving as the blank control. The explants were cultured in 150 mL Erlenmeyer flasks containing 30 mL of liquid MS medium (agar-free) supplemented with 30 $g \cdot L^{-1}$ sucrose at pH 5.8 ± 0.1, under controlled conditions at 21 °C, a 16 h photoperiod, and a light intensity of 2800 lux for 4 weeks. After culture, growth parameters including plant height, fresh weight, dry weight, and leaf number were measured to evaluate the differential growth responses of plants under stress conditions. Another batch of virus-free 4-week-old uniformly grown transgenic and NT plantlets were used for the second experiment (physiological index measurement). Explants were prepared using the same method and cultured in conventional MS liquid medium (without any stress agent) under the identical conditions described above for 4 weeks. Plantlets were subsequently transferred to freshly prepared liquid MS medium supplemented with NaCl (30, 75, or 150 mM) or PEG-6000 (5, 10, or 20% w/v). Plantlets were exposed to drought and salinity for 48 h, during which leaf tissue was harvested at the designated sampling time points. Plantlets maintained in liquid MS medium without NaCl or PEG-6000 over the same period served as controls. A full concentration gradient was employed in this experiment to comprehensively assess the physiological responses under different stress intensities. In a separate experiment, plantlets were exposed to salinity or osmotic stress for 48 h, after which leaf tissue was harvested to determine APX, CAT, SOD, and POD activities, along with H_2O_2 and MDA levels, proline accumulation, and total chlorophyll content.

2.4.*qRT-PCR analysis of StMAPKKKKs expression*

Leaf samples were processed for total RNA isolation using TRIzol reagent (Invitrogen, Carlsbad, CA, USA), following the supplier's recommended procedure. For cDNA preparation, 1 μg of total RNA was treated with DNase and reverse-transcribed using the First-Strand cDNA Synthesis Kit (TransGen Biotech, Beijing, China), according to the manufacturer's protocol. Gene expression following quantitative PCR technique was quantified using SYBR-based amplification in a Roche LightCycler 480 II system (Basel, Switzerland). The assay was set up in a total volume of 20 μL, comprising 10 μL of 2× SYBR Premix Ex Taq (Takara, Japan), cDNA representing 100 ng of starting RNA, and forward and reverse primers, each adjusted to 0.4 μM. The cycling program comprised an initial denaturation at 94 °C for 2 min, followed by 34 cycles of 94 °C for 30 s, 60 °C for 34 s, and 72 °C for 30 s. Transcript levels were normalized against *StEF1α*, and relative expression was determined using the comparative Ct approach ($2^{-\Delta\Delta Ct}$) described by Livak and Schmittgen (2001). For each treatment, nine independent biological replicates were assessed, with each biological replicate run in technical triplicate. Primer sequences for the *StMAPKKKK* genes and *StEF1α* are listed in Supplementary Table S1.

2.5.Subcellular localization analysis of StMAPKKKK1

The full-length open reading frame (ORF) of *StMAPKKKK1* was amplified without the stop codon and cloned upstream of GFP in pCAM35S, yielding the translational fusion 35S:StMAPKKKK1-GFP driven by the CaMV 35S promoter. Transient expression assays were performed in *Nicotiana benthamiana* by *Agrobacterium*-mediated infiltration. The binary vectors pCAM35S-GFP (negative control), 35S:StWRKY75-GFP (positive control; Zhu et al., 2025d), and pCAM35S-GFP-*StMAPKKKK1* were introduced into *Agrobacterium tumefaciens* GV3101, and the resulting transformants were infiltrated into leaves of 5-week-old *N. benthamiana* plants via the abaxial epidermis, essentially as described by Sparkes et al. (2006). After 48 h of incubation at 22 °C in the dark, GFP fluorescence was imaged using an LSM 800 confocal laser-scanning microscope (Carl Zeiss, Jena, Germany). Supplementary Table S1 provides the nucleotide sequences of the primers employed in the cloning experiments.

2.6.Generation of StMAPKKKK1 transgenic potato lines

The full-length CDS of *StMAPKKKK1* was amplified and inserted into pBI121-EGFP (*Xba* I/*Sac* I) downstream of the CaMV 35S promoter to generate the pBI121-EGFP-based *StMAPKKKK1* overexpression vector. The primers (Bioeditas, Shaanxi, China) are listed in Supplementary Table S1, and the assembly was performed according to Li et al. (2020). For RNAi, an *StMAPKKKK1*-specific fragment with terminal *Bam*H I and *Kpn* I sites was cloned into pHANNIBAL in the sense orientation (pHAN-*StMAPKKKK1*-R), after which the corresponding antisense fragment with terminal *Hind* III and *Xba* I sites was inserted into the same plasmid in the antisense orientation to yield pHAN-StMAPKKKK1-RF. The resulting hairpin cassette was excised and subcloned into the binary vector pART using *Bam*H I and *Xba* I, yielding pART-StMAPKKKK1-RNAi, as described by Lu et al. (2019).

To generate the pBI121-EGFP-based *StMAPKKKK1* overexpression vector, the full-length CDS of *StMAPKKKK1* was amplified and inserted downstream of the CaMV 35S promoter into the pBI121-EGFP vector using *Xba* I and *Sac* I restriction sites. The primers (Bioeditas, Shaanxi, China) are detailed in Supplementary Table S1, and the assembly was conducted following the protocol of Li et al. (2020). To construct pHAN-StMAPKKKK1-RF, an StMAPKKKK1-specific fragment containing terminal *BamH* I and *Kpn* I sites was first cloned into pHANNIBAL in the sense orientation to generate pHAN-StMAPKKKK1-R, and subsequently, the corresponding antisense fragment with terminal *Hind* III and *Xba* I sites was inserted into the same plasmid in the antisense orientation. The hairpin cassette was excised and sub-cloned into the binary vector pART using *BamH* I and *Xba* I to generate pART-StMAPKKKK1-RNAi, following the method described by Lu et al. (2019). For plant transformation, LBA4404 cells of *Agrobacterium tumefaciens* were used as hosts for the overexpression and RNA interference (RNAi) plasmids in separate transformation procedures. Bacterial colonies carrying the respective constructs were recovered on LB plates containing 50 mg L^{-1} spectinomycin and 50 mg L^{-1} gentamicin following incubation at 28 °C for two days. A single well-isolated colony was used to inoculate liquid LB medium containing the same antibiotic combination, and the culture was grown overnight at 28 °C with orbital shaking at 220 rpm until the optical density at 600 nm, OD_{600}, reached approximately 0.6. Bacterial cells were harvested by centrifugation at 5,000 × g for 10 min and gently resuspended

in liquid MS medium to give a final OD_{600} of 0.3. Approximately 2-cm stem explants excised from axenic plantlets were immersed in this suspension for 10 min under gentle agitation, briefly blotted to remove excess inoculum, and then placed on co-cultivation medium consisting of MS basal salts adjusted to pH 5.8 and solidified with agar at 7.4 g L^{-1}, together with sucrose at 30 g L^{-1} and the growth regulators IAA at 1.0 mg L^{-1}, GA_3 at 0.2 mg L^{-1}, zeatin, ZT, at 2.0 mg L^{-1} and 6-BA at 0.5 mg L^{-1}; co-cultivation proceeded for 2-3 days in darkness at 22. Following transformation, explants were maintained on shoot-regeneration medium containing 100 mg L^{-1} kanamycin and 300 mg L^{-1} timentin. To sustain regeneration and maintain selection pressure, the explants were transferred to newly prepared medium with identical composition at 14-day intervals.. Kanamycin-resistant shoots were finally rooted on medium at pH 5.8 containing sucrose at 30 g L^{-1}, agar at 7.4 g L^{-1}, kanamycin at 100 mg $L^{-1,}$ and timentin at 300 mg L^{-1}. Putative transgenic lines were screened by PCR using primers specific to the overexpression and RNAi constructs (OE-F/OE-R and RNAi-F/RNAi-R, respectively; Supplementary Table S1). Successful transgene expression was subsequently assessed through qRT-PCR.

2.7.Analysis of protein-protein interactions

2.7.1. The yeast two-hybrid (Y2H) assay

Interactions between StMAPKKKK1 and StMAPKK1–StMAPKK5 were tested with the GAL4-based Matchmaker Two-Hybrid System 3 (Clontech) (Fields and Song, 1989). The full-length CDS of *StMAPKKKK1* was cloned into pGBKT7 (GAL4 BD; *TRP1*), and those of *StMAPKK1–StMAPKK5* into pGADT7 (GAL4 AD; *LEU2*); each CDS was also cloned into the reciprocal vector for bidirectional testing. All constructs were verified by sequencing and co-transformed into *S. cerevisiae* AH109 (*MAT*a; *HIS3*, *ADE2*, *MEL1*, *lacZ*) by the PEG/LiAc/ssDNA method (Gietz and Schiestl, 2007); co-transformants were selected on SD/-TL at 30 °C for 3 d. Auto-activation and toxicity of pGBKT7-*StMAPKKKK1* were assessed by co-transformation with empty pGADT7 on SD/-TLHA plus X-α-Gal, and by comparison of growth on SD/-Trp with that of empty pGBKT7, respectively. Where background growth occurred, assays were repeated on medium containing 3-AT (5, 10, 20, 30, 50, 80 and 100 mM) at the lowest concentration suppressing auto-activation. Tenfold serial dilutions (10^0 to 10^{-3}) were spotted onto SD/-TL and SD/-TLHA with or without X-α-Gal (40 µg mL^{-1}) and incubated at 30 °C for 3–5 d; *HIS3*/*ADE2* activation was scored as growth on SD/-TLHA and *MEL1* activation as blue colonies. Assay performance was validated using the standard interacting pair pGBKT7-53 (murine p53) and pGADT7-T (SV40 large T antigen) as the positive control, whereas the combination of pGBKT7-Lam (human lamin C) and pGADT7-T served as the negative control.

2.7.2. Bimolecular fluorescence complementation (BiFC) assay

To corroborate the interaction between *StMAPKKKK1* and *StMAPKK1–StMAPKK5* in plant cells, we performed BiFC assays by *Agrobacterium*-mediated transient expression in leaves of *Nicotiana benthamiana*, essentially as described by Walter et al. (2004), Sparkes et al. (2006) and Schütze et al. (2009). For BiFC analysis, the complete coding sequence of StMAPKKKK1 was inserted into pSPYCE-35S to produce a fusion with the C-terminal portion of yellow fluorescent protein (YFP). Separately, the coding regions of StMAPKK1 through StMAPKK5 were individually introduced into pSPYNE-35S, each generating a fusion with the N-terminal YFP fragment. Following

sequence verification, the recombinant plasmids were transferred into *Agrobacterium tumefaciens* GV3101. Bacterial transformants were isolated on LB medium supplemented with rifampicin and gentamicin (25 μg·mL^{-1} each), together with the relevant antibiotics required for vector selection. Cultures were grown at 28 °C and 200 rpm to OD_{600} ≈ 1.0; cells were collected by centrifugation (5,000 × *g*, 10 min, 22 °C), resuspended in infiltration buffer (10 mmol·L^{-1} MES-KOH, pH 5.6; 10 mmol·L^{-1} $MgCl_2$; 150 μmol·L^{-1} acetosyringone), adjusted to OD_{600} = 0.8 and incubated at 22 °C in the dark for 2–3 h. Before infiltration, cYFP–StMAPKKKK1 was mixed 1:1 (v/v) with each nYFP–StMAPKK suspension, and a strain expressing the silencing suppressor p19 was added to all mixtures, including controls, at a final OD_{600} of 0.3; cYFP–StMAPKKKK1 with empty pSPYNE-35S served as the negative control. The two uppermost fully expanded leaves of 5-week-old plants were infiltrated using a needle-free 1-mL syringe applied to the abaxial leaf surface, avoiding the midrib. Infiltrated plants were incubated in the dark for 12 h and then transferred to a controlled-environment cabinet maintained at 22 °C and 60–70% relative humidity under a 16 h light/8 h dark photoperiod. At 48 h after infiltration, the infiltrated leaf regions were excised, mounted in water with the abaxial surface uppermost, and imaged using a TCS SP8 laser-scanning confocal microscope from Leica Microsystems, Wetzlar, Germany. YFP was excited at 514 nm, with emission collected over 525–560 nm, whereas chloroplast autofluorescence was recorded with excitation at 633 nm and a detection window of 650–750 nm, allowing plastid-derived signals to be distinguished from genuine complementation-derived YFP fluorescence.

2.7.3. Split-luciferase complementation (SLC) assay

For the SLC assay, the stop-codon-free coding sequences of *StMAP4K1* and *StMAPKK2* were fused to the N- and C-terminal fragments of firefly luciferase in pCAMBIA1300-nLUC and pCAMBIA1300-cLUC (Chen et al., 2008; Zhou et al., 2018). *Agrobacterium tumefaciens* GV3101 carrying the recombinant plasmids was resuspended in infiltration solution containing 10 mM MES-KOH (pH 5.6), 10 mM $MgCl_2$, and 150 μM acetosyringone. The bacterial suspension was standardized to an OD_{600} of 0.8 before infiltration, following Sparkes et al. (2006). Bacterial suspensions carrying the individual constructs were combined in equal proportions immediately before infiltration, and the mixture was infiltrated into leaves of 5-week-old *Nicotiana benthamiana* plants. At 48–60 hpi, leaves were sprayed with 1 mM D-luciferin (0.01% Silwet L-77), dark-adapted for 10 min, and imaged with a cooled-CCD system under identical exposure settings; luminescence from 6-mm leaf discs was measured on a microplate luminometer and expressed as RLU per mm² (Zhou et al., 2018). Empty-vector and reciprocal-tag combinations were included as negative controls, and fusion-protein accumulation was verified by anti-luciferase immunoblotting (Luker et al., 2004; Zhou et al., 2018). Primer information for all constructs is listed in Supplementary Table S1.

2.8. Assessment of Plant Growth Responses to Salinity and Drought Stress

Plant height was measured with a ruler to the nearest 1 mm as the vertical distance from the stem–root junction (where adventitious roots emerge from the main stem) to the apical meristem of the main shoot; the vertical projection was recorded for bent stems. Fresh weight was determined immediately after harvest by removing whole plantlets from the culture vessel, rinsing with deionized water, blotting dry with filter paper, and weighing. Dry weight was determined

according to the method of Qiu et al. (2023) with minor modifications. Enzymatic activity was terminated by exposing the tissue samples to 105 °C for 10 min, after which they were maintained at 80 °C in an oven until no further change in mass was observed. For determination of leaf number, every fully expanded compound leaf on the main shoot and on the two lateral branches was counted, whereas the incompletely expanded leaf at the shoot apex was excluded. Seven genetic lines (one NT line and six transgenic lines) were tested under three treatments, control (liquid MS medium), 30 mM NaCl, and 5% (w/v) PEG-6000, giving 21 line × treatment combinations. Each combination comprised nine independent biological replicates, each consisting of three culture vessels containing one plantlet regenerated from a distinct 2-cm stem explant (567 vessels in total).

2.9. Assessment of Physiological and Biochemical Responses to salinity and drought Stress

To investigate the role of *StMAPKKKK1* in the physiological adaptation of potato to salt and drought stress, a set of biochemical and physiological parameters was quantified under NaCl and PEG-6000 treatments. Activities of antioxidant enzymes were determined spectrophotometrically: ascorbate peroxidase (APX) according to Nakano and Asada (1981), catalase (CAT) according to Aebi (1984), guaiacol peroxidase (POD) according to Maehly and Chance (1954), and superoxide dismutase (SOD) according to Giannopolitis and Ries (1977). H_2O_2 content was measured by the potassium iodide (KI) method of Velikova et al. (2000) as applied by Loreto and Velikova (2001). Malondialdehyde (MDA) content was determined by the thiobarbituric acid (TBA) reaction with correction for soluble-sugar interference (Heath and Packer, 1968; Hodges et al., 1999). Free proline content was quantified using the acid-ninhydrin colorimetric method (Bates et al., 1973) with minor modifications. The content of total chlorophyll in plant tissues was quantified using the BC0990 detection kit supplied by Solarbio (Beijing, China), with measurements performed according to the kit's prescribed instructions. Detailed protocols for all measurements are provided in Supplementary Data 1. For these measurements, the same seven genetic lines (one NT line and six transgenic lines) were used. Each line was subjected to one control condition (liquid MS medium without stress agents) and six stress treatments (NaCl at 30, 75 and 150 mM; PEG-6000 at 5%, 10% and 20%, w/v), giving 49 line × treatment combinations. Each combination comprised nine biological replicates, each consisting of three culture bottles, and each bottle contained three plantlets regenerated from separate 2-cm stem explants, giving 1,323 culture bottles in total.

2.10. **Statistical analysis**

All data were analyzed using GraphPad Prism 9.0 (GraphPad Software, San Diego, CA, USA) and IBM SPSS Statistics 19.0 (IBM Corp., Chicago, IL, USA). Each treatment comprised nine independent biological replicates (n = 9), and values are presented as mean ± standard deviation (SD). Differences among experimental groups were examined by two-way analysis of variance (ANOVA), and Tukey's honestly significant difference (HSD) procedure was applied for subsequent pairwise mean separations. Probability thresholds of 0.05, 0.01 and 0.001 were adopted as the criteria for statistical significance and are indicated by one, two and three asterisks, respectively (*$P < 0.05$; **$P < 0.01$; ***$P < 0.001$). All figure panels were assembled using Adobe Illustrator 2022 (Adobe Inc., San Jose, CA, USA).

3. Results

3.1.Bioinformatics analysis

3.1.1. Genome-Wide Identification and Molecular Characterization of the Potato StMAPKKKK Gene Family

Eight *StMAPKKKK* members were identified in the potato genome and designated *StMAPKKKK1* to *StMAPKKKK8* according to ascending chromosome number and genomic position. All eight proteins contained the characteristic MAP4K kinase motifs: the glycine-rich motif GxGxxG/A, the invariant lysine of the ATP-binding site, the HRD and DFG motifs of the activation loop, and the MAP4K signature VGTPxWMAPEv (Fig. S1). The eight genes were non-randomly distributed across six of the twelve potato chromosomes (Chr02, Chr03, Chr05, Chr06, Chr07 and Chr08) (Fig. S2). Two members were located on Chr06 (*StMAPKKKK4* and *StMAPKKKK5*) and two on Chr08 (*StMAPKKKK7* and *StMAPKKKK8*), whereas single members occurred on Chr02 (*StMAPKKKK1*), Chr03 (*StMAPKKKK2*), Chr05 (*StMAPKKKK3*) and Chr07 (*StMAPKKKK6*); none were detected on Chr01, Chr04 or Chr09–Chr12. Genes were present on both strands, indicating a dispersed and uneven genomic distribution. The predicted proteins varied considerably in physicochemical properties. Amino acid length ranged from 523 (*StMAPKKKK4*) to 815 (*StMAPKKKK3*) residues, with corresponding molecular weights of 58,788.95 to 89,891.76 Da. Theoretical pI values ranged from 4.92 to 6.55, indicating weak acidity; instability indices ranged from 44.48 to 55.36, classifying all members as unstable; aliphatic indices ranged from 70.93 to 85.16, suggesting relatively high thermostability. All proteins had negative GRAVY values (−0.627 to −0.359), identifying them as hydrophilic, with *StMAPKKKK6* the most and *StMAPKKKK4* the least hydrophilic. Detailed annotation of each gene, including gene ID, family classification, chromosomal assignment, genomic coordinates, and strand orientation, is given in Table S2.

3.1.2. Phylogenetic analysis of the StMAPKKKKs

An unrooted neighbour-joining (NJ) tree was constructed from the full-length amino acid sequences of 25 MAPKKKK proteins—8 StMAPKKKK from *Solanum tuberosum* (potato), 10 AtMAP4K from *Arabidopsis thaliana* and 7 OsMAP4K from *Oryza sativa* (rice)—and displayed in circular form (Fig. 1). Based on tree topology, sequence homology and the established *Arabidopsis* classification, the proteins were divided into three major clades (I–III); Clade III was the largest and was further resolved into four well-supported subclades, III-A to III-D. The potato members were distributed as follows: StMAPKKKK6 in Clade I; StMAPKKKK3 in Clade II; StMAPKKKK2 and StMAPKKKK5 in III-A; StMAPKKKK1 in III-B; StMAPKKKK7 and StMAPKKKK8 in III-C; and StMAPKKKK4 in III-D (Fig. 1; Table S3).

Homologues from the two dicots (potato and *Arabidopsis*) and the monocot (rice) were intermingled throughout the tree, indicating that the MAP4K family has remained highly conserved among these species without large-scale lineage-specific gene loss. The StMAPKKKK proteins showed closer affinity to AtMAP4K than to OsMAP4K, consistent with both being dicots; StMAPKKKK6, for example, grouped tightly with AtMAP4K1 and AtMAP4K2 within Clade I, suggesting conserved roles in related signalling pathways. Gene nomenclature, subfamily

classification, gene IDs, and protein sequences of all MAP4K members from the three species are listed in Table S3.

3.1.3. Gene structure and conserved protein motif analysis of StMAPKKKKs

Gene structure varied substantially among the eight *StMAPKKKK* members, with exon number ranging from 1 to 22 (Fig. 2A). *StMAPKKKK8* had the highest exon count (22), followed by *StMAPKKKK7* (21), *StMAPKKKK1*, *StMAPKKKK5* and *StMAPKKKK6* (20 each) and *StMAPKKKK3* (18). *StMAPKKKK4* was the exception, consisting of a single exon with no introns. Genomic length also differed markedly among members, ranging from approximately 1,700 to 17,000 bps. Most multi-exon genes carried UTRs at both ends, whereas *StMAPKKKK2* and *StMAPKKKK5* retained only short 3′ UTR fragments. The extensive intron insertions in multi-exon members accounted for their greater genomic lengths, indicating that intron gain/loss events during evolution contributed to the structural divergence of this family.

Conserved motifs in the eight StMAPKKKK proteins were analyzed using MEME, which identified 20 motifs (motifs 1–20) across the full-length protein sequences; the consensus sequence logos are shown in Fig. S3. Motif number varied considerably among members, ranging from 5 to 17 (Fig. 2B): StMAPKKKK2 and StMAPKKKK5 contained 17 motifs, the most complete composition; StMAPKKKK7 and StMAPKKKK8 had 15 each; StMAPKKKK1 had 13; StMAPKKKK4 had 7; StMAPKKKK3 had 6; and StMAPKKKK6 had the fewest, with 5. Comparison of motif arrangement revealed both conserved and member-specific features. Motifs 1–5 were present in all eight proteins. By contrast, motifs 15, 19 and 20 occurred exclusively in StMAPKKKK2 and StMAPKKKK5; motifs 12, 16 and 17 only in StMAPKKKK7 and StMAPKKKK8; and motifs 7, 9 and 10 were present in most members but absent from StMAPKKKK3 and StMAPKKKK6 (Fig. 2B). Together, these results indicate that the family combines a conserved core motif set, suggestive of functional conservation, with member-specific motifs that may underlie functional diversification.

3.1.4. Gene duplication, collinearity, and promoter cis-element analyses of the StMAPKKKKs

MCScanX was used to identify duplication events within the *StMAPKKKK* gene family. Two segmentally duplicated gene pairs were detected among the 8 members: *StMAPKKKK2–StMAPKKKK5*, located on chromosomes 3 and 6, and *StMAPKKKK7–StMAPKKKK8*, both located on chromosome 8 (Fig. S4). The Ka/Ks ratios of both duplicated pairs were below 1 (*StMAPKKKK2*/*StMAPKKKK5*, 0.281; *StMAPKKKK7*/*StMAPKKKK8*, 0.204; Table S4), indicating that they have been subjected to purifying selection. Interspecific synteny analysis identified eight collinear gene pairs between potato and *Arabidopsis*, involving five *StMAPKKKK* genes and seven *Arabidopsis* homologues (Fig. S5; Table S5). By contrast, only two collinear pairs were detected between potato and rice, involving two *StMAPKKKK* genes and two rice homologues (Table S5).

Putative cis-acting regulatory elements (CREs) in the 2-kb upstream regions of the *StMAPKKKK* genes were identified with PlantCARE. In total, 775 CREs were detected and assigned to five functional categories—core promoter, light-responsive, phytohormone-responsive, stress-responsive, and growth- and development-related elements—based on the functional annotations

provided by PlantCARE (Fig. S6; Table S6). Core promoter elements were the most abundant (582, 75.1%), consisting mainly of TATA-box (458) and CAAT-box (122), together with a few CCAAT-box and A-box motifs; their number varied considerably among members, from 109 in *StMAPKKKK2* to 42 in *StMAPKKKK8*. Light-responsive elements were the largest group among the environmentally regulated categories (81, 10.45%), comprising 14 motif types including AE-box, Box4, G-box, MRE and GT1-motif, and were present in all eight promoters, suggesting that light signalling is an important environmental input for this family, which may participate in photomorphogenesis and light-coordinated stress responses. Phytohormone-responsive elements totaled 59 (7.6%) and covered five hormone signalling pathways: MeJA-responsive elements (CGTCA- and TGACG-motifs; 32, with the highest number in *StMAPKKKK7*, 10); ABA-responsive elements (ABRE; 14, present in all promoters except that of *StMAPKKKK3*); auxin-responsive elements (TGA-element and AuxRR-core; 6); gibberellin-responsive elements (GARE-motif, TATC-box and P-box; 4); and salicylic acid-responsive elements (TCA-element; 3). This indicates broad involvement of the family in hormone-mediated signalling, particularly ABA-dependent abiotic stress responses and jasmonate-mediated defence. Stress-responsive elements numbered 30 (3.9%). The drought-induced MYB-binding site MBS (13) was present in all eight promoters, indicating a general capacity for drought response, whereas ARE and GC-motif involved in anaerobic induction totalled 12; LTR (low temperature) and the WUN-motif (wounding) were each represented once, in *StMAPKKKK3* and *StMAPKKKK4*, respectively; and TC-rich defence/stress repeats (3) occurred in *StMAPKKKK1* and *StMAPKKKK8*. These results suggest a shared drought responsiveness together with functional differentiation among members in responses to low temperature and wounding. Growth/development-related elements were the least abundant (23, 2.95%) and included CAT-box (meristem expression), circadian, the ATBP-1 binding site, MBSI (flavonoid biosynthesis) and the O_2-site (prolamin metabolism) (Fig. S6; Table S6), suggesting that some members may contribute to meristem development, circadian maintenance and secondary metabolic regulation. Together, these results indicate that *StMAPKKKK* transcription is potentially coordinated by basal promoter elements, light signals, multiple phytohormones and external stress cues, with functions spanning normal growth and development as well as abiotic stress signalling, notably drought response.

3.2.Expression patterns of StMAPKKKK genes in potato leaves following salinity and drought treatments

The transcriptional responses of the eight *StMAPKKKK* genes to salinity were examined by qRT-PCR using leaf tissues of potato cv. *'Atlantic'* collected at multiple time points from 0 to 48 h following treatment with 30, 75 or 150 mM NaCl (Fig. 3A–H). Among the eight members, *StMAPKKKK1* exhibited the strongest and most persistent upregulation, with transcript levels increasing markedly in parallel with rising NaCl concentrations; peak accumulation occurred at 16 h under 150 mM NaCl, after which expression declined slightly at 24 h but remained at a relatively high level at 48 h (Fig. 3A). In contrast, *StMAPKKKK3*, *StMAPKKKK4* and *StMAPKKKK6* displayed low sensitivity to 30 mM NaCl, showing no significant differences in expression relative to the 0 h control at multiple time points from 1 to 48 h, particularly at 48 h (Fig. 3C–D, F). Similarly, *StMAPKKKK2*, *StMAPKKKK3* and *StMAPKKKK4* exhibited relatively low sensitivity to 75 mM NaCl, with weak induction and no significant differences from the 0 h control at multiple

time points, especially at 48 h (Fig. 3B–D). Furthermore, *StMAPKKKK2*, *StMAPKKKK3*, *StMAPKKKK4* and *StMAPKKKK6* did not show obvious induced expression at multiple time points (1–48 h) under 150 mM NaCl (Fig. 3B–D, F). By comparison, *StMAPKKKK5*, *StMAPKKKK7* and *StMAPKKKK8* displayed salt-regulated induced expression patterns, showing significant upregulation under all three salt concentrations, with more pronounced induction under severe salt stress (150 mM) at various time intervals, albeit at lower intensities than those of *StMAPKKKK1* (Fig. 3E, G–H). Collectively, these results revealed differential salt sensitivity among *StMAPKKKK* members, wherein *StMAPKKKK1*, *StMAPKKKK5*, *StMAPKKKK7* and *StMAPKKKK8* exhibited induced expression patterns under all three salt treatments, and *StMAPKKKK1* was the most stably and highly induced gene across different time points. Similarly, to characterize the transcriptional response of the family to drought stress, relative expression levels were measured in leaves of cv. *'Atlantic'* subjected to 5%, 10% and 20% PEG-6000 over a 0–48 h time course (Fig. 4A–H). *StMAPKKKK1* exhibited significant upregulation under all three PEG-6000 concentrations, with induction magnitude increasing progressively with PEG concentration; under 20% PEG-6000, transcript levels accumulated rapidly from 1 to 16 h, remained at the highest relative levels from 24 to 48 h and reached the absolute peak at 48 h (Fig. 4A). *StMAPKKKK2* and *StMAPKKKK6* showed significant induction only at middle-to-late stages (8, 16 and 24 h) under 20% PEG-6000, whereas their responses were weak and non-significant at multiple time points under 5% and 10% PEG-6000 (Fig. 4B, F). *StMAPKKKK3* peaked at 4 h under 20% PEG-6000, with significant induction persisting at later time points (8, 16, 24 and 48 h) but declining relative to the 4 h peak; under 5% PEG-6000 its response was weak and non-significant at 2, 4 and 16 h, and under 10% PEG-6000 it was non-significant at early stages (1 and 2 h), with upregulation restricted to middle-to-late stages and limited fluctuation across time points (Fig. 4C). *StMAPKKKK4* and *StMAPKKKK7* exhibited weak, non-significant responses at multiple time points under all three PEG-6000 concentrations, even at 48 h under 20% PEG-6000 (Fig. 4D, G). In contrast, *StMAPKKKK5* and *StMAPKKKK8* displayed significant, dose-dependent upregulation under all three treatments, with transcripts accumulating steadily with minor fluctuations from 1 to 8 h, peaking at 16 h and remaining relatively high at 24 and 48 h (Fig. 4E, H). In summary, *StMAPKKKK1*, *StMAPKKKK5* and *StMAPKKKK8* exhibited drought-regulated induction patterns across the three PEG-6000 treatments, with *StMAPKKKK1* showing the most stable and highest induction among family members.

3.3.Tissue-specific expression of StMAPKKKKs

Transcript abundance of the eight *StMAPKKKK* genes was examined in five potato organs (root, stem, leaf, flower and tuber), and each gene showed a distinct tissue-preferential pattern (Fig. S7). *StMAPKKKK1* and *StMAPKKKK5* were preferentially expressed in leaves, with moderate expression in roots. *StMAPKKKK3*, *StMAPKKKK6*, *StMAPKKKK7* and *StMAPKKKK8* showed root-preferential expression; among these, *StMAPKKKK3* and *StMAPKKKK7* had the highest transcript accumulation in roots followed by tubers, whereas *StMAPKKKK8* was highest in roots followed by leaves. *StMAPKKKK2* and *StMAPKKKK4* maintained low abundance in all tissues examined, with no significant differences among most tissues. These results indicate functional diversification within the family and suggest roles for the root-preferential members in root growth and development, and for *StMAPKKKK1* and *StMAPKKKK5* in leaf-associated processes.

3.4.Generation and molecular verification of StMAPKKKK1 transgenic plants

To examine the function of *StMAPKKKK1* in potato salt and drought tolerance, stable OE and RNAi lines were generated in cv. *'Atlantic'*. Integration of the overexpression and RNAi constructs was confirmed by RT-PCR (Fig. S8A, B). Transcript abundance of *StMAPKKKK1* in independent transgenic lines was then quantified by qRT-PCR: relative to NT plants, *StMAPKKKK1* levels were markedly increased in OE lines (~17-fold; ***$P < 0.001$; Fig. S8C) and significantly reduced in RNAi lines by 78% (***$P < 0.001$; Fig. S8D). Based on these results, three OE lines with the highest transcript accumulation (OE-1, OE-2 and OE-4) and three RNAi lines with the strongest silencing (RNAi-2, RNAi-3 and RNAi-4) were selected for subsequent phenotypic, physiological and molecular analyses under both stress conditions.

3.5.Subcellular localization analysis of StMAPKKKK1 via transient expression

The subcellular localization of StMAPKKKK1 was examined by transient expression of a GFP fusion in *Nicotiana benthamiana* leaf epidermal cells, with free GFP as a control and a GFP–StWRKY75 fusion as a nuclear localization marker (Fig. 5). No specific subcellular localization was observed for free GFP; its fluorescence was spread across the cell membrane, cytoplasm, and nucleus) in a pattern typical of a freely diffusing protein. The nuclear marker GFP–StWRKY75 was detected exclusively in the nucleus. In cells expressing GFP–StMAPKKKK1, fluorescence was observed at the plasma membrane and in the cytoplasm, with no apparent co-localization with chloroplast autofluorescence (Fig. 5). The results suggest that StMAPKKKK1 is distributed between the cell membrane and cytoplasm under the experimental conditions examined.

3.6.StMAPKKKK1 interacts specifically with StMAPKK2

To identify downstream partners of StMAPKKKK1, its interactions with the five potato MAPKKs (StMAPKK1–StMAPKK5) were screened by a GAL4-based yeast two-hybrid (Y2H) assay. All bait–prey combinations grew comparably on non-selective SD/−TL medium, confirming co-transformation (Fig. 6A, B). On selective SD/−TLHA medium, yeast co-expressing StMAPKKKK1-BD and StMAPKK2-AD grew at the undiluted density and retained growth at the 10^{-1} dilution, whereas no growth occurred with StMAPKK1, StMAPKK3, StMAPKK4 or StMAPKK5 (Fig. 6A). Activation of the *MEL1* reporter corroborated this: colonies of StMAPKKKK1-BD + StMAPKK2-AD turned blue on SD/−TLHA supplemented with X-α-Gal (Fig. 6A, right panel). Reciprocal testing (StMAPKK1–StMAPKK5-BD × StMAPKKKK1-AD) gave an identical pattern, with growth and blue coloration restricted to StMAPKK2-BD + StMAPKKKK1-AD (Fig. 6B). The pGBKT7-53/pGADT7-T positive control grew as blue colonies on selective medium, whereas the pGBKT7-Lam/pGADT7-T negative control failed to grow on selective medium (Fig. 6A, B). The interaction between StMAPKKKK1 and StMAPKK2 was further validated in leaf epidermal cells of *Nicotiana benthamiana* using a BiFC assay, in which reconstituted YFP fluorescence was detected. YFP fluorescence was detected only in cells co-expressing cYFP-StMAPKKKK1 and nYFP-StMAPKK2, and not with nYFP-StMAPKK1, nYFP-StMAPKK3, nYFP-StMAPKK4, nYFP-StMAPKK5 or the empty nYFP vector (Fig. 6C). In the positive combination, the YFP signal was distributed at the cell periphery and in the cytoplasm, consistent with the subcellular localization of StMAPKKKK1; chlorophyll

autofluorescence, recorded in a separate channel, showed no overlap with the YFP signal (Fig. 6C, Merge). The interaction was independently confirmed by split-luciferase complementation imaging in *N. benthamiana* leaves. Strong luminescence was detected specifically in the sector co-infiltrated with cLUC-StMAPKKKK1 and nLUC-StMAPKK2 (Fig. 6D, lower-left quadrant), whereas the three control sectors, cLUC-StMAPKKKK1 + empty nLUC (upper-left), empty cLUC + nLUC-StMAPKK2 (upper-right) and cLUC-StMAPKKKK1+nLUC-StMAPKK1 (lower-right), showed only background-level luminescence (Fig. 6D); in the color scale, red/yellow and blue indicate high and low relative luminescence intensity, respectively. Together, three independent assays, bidirectional Y2H, BiFC and split-luciferase complementation, consistently showed that StMAPKKKK1 associates specifically with StMAPKK2, but not with StMAPKK1, StMAPKK3, StMAPKK4 or StMAPKK5.

Based on this specific physical association, we next asked whether *StMAPKKKK1* influences *StMAPKK2* transcript abundance in transgenic potato plants under normal and stress conditions. Under control (non-stress) conditions, *StMAPKK2* transcript levels were comparable among NT, *StMAPKKKK1*-OE and *StMAPKKKK1*-RNAi lines, indicating that altered *StMAPKKKK1* expression has little effect on basal *StMAPKK2* transcript abundance. Following NaCl treatment, *StMAPKK2* expression was induced in all genotypes, but the magnitude of induction differed: transcript levels were consistently higher in OE lines and lower in RNAi lines than in NT plants, and the difference became more pronounced as the NaCl concentration increased, being greatest at 150 mM NaCl (Fig. S9). A similar pattern was observed under PEG-6000-induced osmotic stress, where *StMAPKK2* transcript abundance was higher in OE lines and lower in RNAi lines relative to NT plants, with the largest differences at the highest PEG-6000 concentration (Fig. S9). These results suggest that *StMAPKKKK1* positively modulates the stress-responsive induction of *StMAPKK2* transcription under salt and osmotic stress.

3.7.StMAPKKKK1 positively regulates potato growth under salt and drought stress

The physiological role of *StMAPKKKK1* was analyzed *in vitro* using potato cv. *'Atlantic'* plantlets comprising NT, three OE lines (OE-1/2/4), and three RNAi lines (RNAi-2/3/4) were cultured for 4 weeks in liquid MS medium without or with 30 mM NaCl or 5% PEG-6000 (Fig. 7A–E). Under control conditions, OE lines grew better than NT whereas RNAi lines grew worse; both stresses inhibited growth in all lines, but OE lines showed the least damage and better shoot and root development, whereas RNAi lines exhibited pronounced dwarfing and growth inhibition (Fig. 7A). Plant height (Fig. 7B) exceeded that of NT in OE-1 and OE-2 under control conditions but not in OE-4, and was lower in RNAi-2 and RNAi-3 but not in RNAi-4; under salt stress only OE-1 exceeded NT whereas all RNAi lines were shorter, and under drought stress OE-1 and OE-4 were taller whereas RNAi-3 and RNAi-4 were shorter. For fresh weight (Fig. 7C), OE lines exceeded NT and RNAi-2 and RNAi-3 were lower than NT (RNAi-4 not significant) under control conditions; salt stress reduced fresh weight in all lines, with OE-1 and OE-2 higher and OE-4 unchanged relative to NT and all RNAi lines lower, whereas under drought stress OE-1 and OE-4 were higher and OE-2 unchanged, and only RNAi-2 was comparable to NT among the RNAi lines. Dry weight (Fig. 7D) was higher in all OE lines than NT under control and both stress conditions, and lower in all RNAi lines under control and salt conditions; under drought stress, RNAi-2 was

unchanged whereas RNAi-3 and RNAi-4 were lower. Leaf number (Fig. 7E) did not differ from NT under control conditions except in OE-2 and OE-4, which had more leaves, and was higher in all OE lines under both stresses, whereas RNAi lines did not differ from NT under salt stress and only RNAi-3 had fewer leaves under drought stress. Together, these results show that *StMAPKKKK1* overexpression mitigates the growth inhibition imposed by salt and drought stress, as reflected in superior leaf retention, plant height, and biomass accumulation, whereas its suppression exacerbates it.

3.8.StMAPKKKK1 enhances antioxidant enzyme activities under salt and drought stress

To assess whether *StMAPKKKK1* contributes to ROS scavenging under salinity and drought stress, we quantified the activities of four major antioxidant enzymes (APX, CAT, SOD, and POD) in NT lines, *StMAPKKKK1*-OE lines (OE-1/2/4), and RNAi-mediated knockdown lines (RNAi-2/3/4) (Fig. 8A–D). Under non-stressed conditions, no statistically significant variation ($P > 0.05$) in APX, CAT, SOD, or POD activity was detected among these genotypes, indicating that altered *StMAPKKKK1* expression does not perturb the basal antioxidant capacity in the absence of environmental stress. Relative to the corresponding untreated controls, the activities of all four enzymes increased markedly in every line tested after exposure to salt stress (30, 75, and 150 mM NaCl) or drought stress simulated with PEG-6000 (5%, 10% and 20%, w/v), although the magnitude of induction differed substantially among lines. Under all stress treatments, the OE lines consistently exhibited significantly higher APX activity than NT plants ($*P < 0.05$, $**P < 0.01$, $***P < 0.001$), whereas the RNAi lines displayed substantially lower APX activity ($*P < 0.05$, $**P < 0.01$, $***P < 0.001$), reflecting a reduced capacity to eliminate ROS (Fig. 8A). A similar trend was observed for CAT activity, with OE lines showing significantly greater enzymatic activity ($*P < 0.05$, $**P < 0.01$, $***P < 0.001$) than NT plants under both salinity and drought stress, whereas RNAi-mediated suppression of *StMAPKKKK1* resulted in a pronounced decline (Fig. 8B). Likewise, SOD activity was markedly elevated ($*P < 0.05$, $**P < 0.01$, $***P < 0.001$) in the OE lines compared with NT controls under all salt and drought treatments, whereas RNAi plants exhibited significantly lower SOD activity ($*P < 0.05$, $**P < 0.01$, $***P < 0.001$), indicating impaired conversion of superoxide radicals into hydrogen peroxide (Fig. 8C). Consistent with these observations, POD activity was also significantly enhanced ($*P < 0.05$, $**P < 0.01$, $***P < 0.001$) in *StMAPKKKK1*-overexpressing plants but markedly reduced in the RNAi lines under both stress conditions (Fig. 8D). The coordinated upregulation of APX, CAT, SOD and POD activities in the OE lines, together with their suppression in the RNAi plants, indicates that *StMAPKKKK1* positively modulates the antioxidant defense system under drought and salt stress, and that enhanced ROS-scavenging capacity contributes to the improved abiotic stress tolerance of potato.

3.9.StMAPKKKK1 mediates physiological adaptations to salt and drought stress in potato

To assess the involvement of *StMAPKKKK1* in stress resilience, H_2O_2, MDA, proline and total chlorophyll contents were determined in NT, OE (OE-1/2/4) and RNAi (RNAi-2/3/4) lines under control conditions and across salinity (30, 75 and 150 mM NaCl) and PEG-6000 (5%, 10% and 20%) gradients (Fig. 9A–D). Under non-stress conditions, none of the four parameters differed significantly among genotypes, indicating that altered *StMAPKKKK1* expression does not affect basal physiological homeostasis. Stress increased H_2O_2 accumulation in all genotypes, but the

extent differed with *StMAPKKKK1* level: H_2O_2 was consistently lower in OE lines and higher in RNAi lines than in NT across all treatments, indicating that overexpression limits stress-induced ROS accumulation whereas suppression disturbs redox homeostasis (Fig. 9A). MDA showed a comparable pattern: although salt and drought increased membrane lipid peroxidation in all lines, the increase was attenuated in OE lines and amplified in RNAi lines, suggesting that *StMAPKKKK1* contributes to the maintenance of membrane integrity (Fig. 9B). Proline accumulation paralleled *StMAPKKKK1* expression, being higher in OE lines and lower in RNAi lines than in NT under both stresses, consistent with improved osmotic adjustment in OE plants (Fig. 9C). Total chlorophyll declined progressively under both stresses; this decline was smaller in OE lines and greater in RNAi lines than in NT, indicating that *StMAPKKKK1* favors the retention of photosynthetic pigments under stress (Fig. 9D). Together, these results indicate that *StMAPKKKK1* improves physiological performance under salt and drought stress by limiting oxidative damage, maintaining membrane integrity, promoting proline-associated osmotic adjustment and delaying chlorophyll loss.

4. Discussion

This study presents a genome-wide investigation of the potato MAPKKKK gene family, identifying eight StMAPKKKK members and characterizing their molecular features. These findings provide an evolutionary perspective on this kinase family and a foundation for further elucidating its biological functions and potential contributions to abiotic stress responses. The family size is comparable to those of *Arabidopsis thaliana* and rice (Champion et al., 2004; Pan et al., 2021) but smaller than those of maize (He et al., 2026), wheat (Li et al., 2024b) and cotton (Zeng et al., 2025), reflecting both the evolutionary conservation and the lineage-specific expansion of MAP4Ks among plant species; genome-wide identification has been reported in *A. thaliana* (Ichimura et al., 2002; Champion et al., 2004), *Oryza sativa* and other green-lineage species (Pan et al., 2021), *Zea mays* (He et al., 2026), *Triticum aestivum* (Li et al., 2024b) and *Gossypium hirsutum* (Zeng et al., 2025), revealing their conservation and roles in growth, development and abiotic stress responses (Jonak et al., 2002; Li et al., 2024b; Zeng et al., 2025; Ren et al., 2026; He et al., 2026), whereas a comprehensive analysis in potato has been unavailable.

Phylogenetic analysis resolved the potato MAP4K family into three major clades (Fig. 1), closely resembling and consistent with the classifications reported for Arabidopsis, wheat, maize and cotton and indicating that the tripartite structure of plant MAP4Ks has been highly conserved since the monocot–dicot divergence (Jonak et al., 2002; Li et al., 2024b; Zeng et al., 2025; He et al., 2026); all StMAPKKKK proteins retain the characteristic catalytic kinase motifs, a glycine-rich ATP-binding motif, a conserved lysine, the HRD and DFG activation-loop motifs and the MAP4K-specific VGTPxWMAPEv signature (Fig. S1), indicating that the catalytic core has been subject to strong evolutionary constraint as in wheat and cotton MAP4Ks (Li et al., 2024b; Zeng et al., 2025), whereas the marked inter-subfamily variation in exon–intron organization and motif composition (Fig. 2; Fig. S3) reflects divergence in regulatory patterns and protein architecture rather than alteration of catalytic activity. Only eight members were identified, distributed across six of the twelve chromosomes (Table S2; Fig. S2), far fewer than in wheat and cotton; this difference is partly attributable to ploidy, because this study used the chromosome-scale, single-

haplotype reference genome DM v6.1 of *Solanum tuberosum* Group Phureja doubled monoploid clone DM1-3 516 R44, generated by Oxford Nanopore long-read sequencing with Hi-C scaffolding (Pham et al., 2020), which, owing to its highly homozygous background, circumvents the extreme heterozygosity of tetraploid cultivated potato (*Solanum tuberosum*, 2n = 4x = 48), whereas the larger wheat (hexaploid) and cotton (allotetraploid) families reflect the gene redundancy inherent in polyploid genomes. Consistently, synteny analysis detected only two segmental duplication events and no tandem duplications (Fig. S4), indicating extremely limited expansion in potato, in contrast to the extensive duplication and duplicate retention in wheat and cotton that implicate recent polyploidization as a key driver of family expansion (Li et al., 2024b; Zeng et al., 2025). Both duplicated pairs had Ka/Ks ratios < 1 (Table S4), indicating strong purifying selection with constrained coding sequences and elimination of deleterious substitutions; this is corroborated by the intact catalytic motifs of all StMAPKKKK proteins, indicating that sequence variation is concentrated in non-catalytic regions, shaping subfamily differences in gene structure and motif composition and facilitating divergence in regulatory modes rather than loss of catalytic activity. Nevertheless, the duplicated members and other *StMAPKKKKs* displayed markedly distinct tissue-specific (Fig. S7) and stress-responsive (Figs. 3, 4 and S7) expression profiles, indicating functional differentiation that we hypothesize is attributable to diverse promoter cis-elements.

Promoter analysis showed that *StMAPKKKK* promoters harbor abundant ABRE, MBS and MeJA-responsive elements (Fig. S6; Table S6), consistent with the enrichment of ABA-, drought- and JA-responsive cis-elements in wheat MAPKKKK promoters (Li et al., 2024b) and with correlations between promoter architecture and stress-inducible expression in cotton (Zeng et al., 2025); these elements correspond to the transcriptional profiles, since *StMAPKKKK1*, the most strongly induced member under salt and drought (Fig. 3A and 4A), contains two ABRE and three MBS elements, the highest enrichment in the family, providing a cis-regulatory basis for its rapid activation and suggesting cooperative regulation by ABA-responsive bZIP transcription factors and stress-induced MYB proteins, whereas the root-preferential expression of *StMAPKKKK3*, *StMAPKKKK6*, *StMAPKKKK7* and *StMAPKKKK8* (Fig. S7) is associated with development-related elements such as the CAT-box, reflecting regulatory specialization toward root functions. Thus, despite limited expansion, promoter sequence divergence constitutes an important evolutionary mechanism underlying the functional specialization of individual members during adaptation to abiotic stress, and the stress-responsive patterns, mutually corroborated by promoter characteristics, further support a conserved role of MAPKKKKs in abiotic stress signalling. Comparisons show that cotton *GhMAPKKKKs*, particularly *GhMAPKKKK13*, positively regulate salinity and drought tolerance (Zeng et al., 2025) and *Arabidopsis* MAP4K1/MAP4K2 are activated by OST1-dependent phosphorylation during drought and ABA signalling (Tang et al., 2025; Hu et al., 2026), whereas pepper *CaMAP4K3* negatively regulates drought resistance (Lim et al., 2025); consistent with a conserved yet functionally diversifying role, the *StMAPKKKK* genes showed differential expression under salt and drought (Fig. 3, 4) and distinct tissue-specific patterns (Fig. S7), and *StMAPKKKK1* increased progressively with stress duration and intensity, peaking at 16 h under 150 mM NaCl and at 48 h under 20% PEG (Fig. 3, 4). Unlike *CaMAP4K3,* *StMAPKKKK1* was demonstrated here to positively regulate both salt and drought tolerance, indicating that although MAPKKKK/MAP4K proteins are conserved components of plant stress-

signalling networks, their downstream functions and effects on tolerance are not necessarily conserved, highlighting species- and member-specific diversification; on this basis, *StMAPKKKK1* was selected for functional characterization.

Subcellular localization, which indicates the compartments where signalling is perceived, transmitted and regulated (Komis et al., 2018), showed that StMAPKKKK1 localizes predominantly to the cell membrane and cytoplasm (Fig. 5), suggesting a role in stress signal perception and early extracellular signal transmission as well as in interactions with downstream components for intracellular relay, although localization alone does not establish specific compartment functions; this distribution matches those of Arabidopsis AtMAPKKKK4 (SIK1) (Jiang et al., 2019), AtMAPKKKK1 and AtMAPKKKK2 (Tang et al., 2025; Hu et al., 2026) and rice OsMAPKKKK6 (Ren et al., 2026), supporting involvement in membrane-associated and cytoplasmic stress signalling, and provides a spatial context for its physical association with StMAPKK2, verified by Y2H, BiFC and SLC assays (Fig. 6A–D), with the reconstituted YFP signal of the StMAPKKKK1–StMAPKK2 pair localizing to the plasma membrane/cortical region and showing no nuclear enrichment (Fig. 6C), indicating that the association occurs primarily at or near the plasma membrane, although whether it is dynamically redistributed under stress is unknown. As documented for *Arabidopsis* MAP4K1 with SLAC1 and OST1 (Tang et al., 2025), such interactions can be associated with phosphorylation-dependent signalling; nevertheless, because phosphorylation of StMAPKK2 by StMAPKKKK1 was not directly examined, the interaction should be interpreted as evidence of physical association rather than kinase–substrate activity. Moreover, StMAPKKKK1 physically interacts with StMAPKK2, and *StMAPKK2* exhibits a stress-responsive expression pattern in *StMAPKKKK1*-OE and RNAi lines. These findings indicate that the StMAPKKKK1 and StMAPKK2 signaling module participates in plant stress responses. However, whether this pathway mediates stress responses through StMAPKKKK1-dependent phosphorylation of StMAPKK2, and how StMAPKKKK1 regulates downstream targets, remain to be fully elucidated.

Maintenance of growth under adverse conditions is a key component of adaptation, requiring a balance between protective mechanisms and continued growth (Bechtold and Field, 2018), and MAP4Ks are increasingly recognized as upstream signalling hubs coordinating stress perception with growth and adaptation, as exemplified by favorable *ZmMAP4K2*/*ZmMAP4K4* alleles in maize (He et al., 2026) and by *Arabidopsis* MAP4K1/MAP4K2 acting downstream of OST1 to regulate ABA-mediated drought responses through phosphorylation of guard-cell targets (Hu et al., 2026). Consistent with this, *StMAPKKKK1* overexpression improved plant height, fresh weight and dry weight under both salt and drought stress (Fig. 7) and also affected growth parameters under non-stress conditions, indicating enhanced tolerance together with maintained growth; because StMAPKKKK1 contains conserved serine/threonine kinase motifs, these effects may reflect phosphorylation-dependent signalling, although its kinase activity and downstream phosphorylation targets were not investigated and require validation. Although plant MAP4Ks remain less understood than the canonical MAPK cascade, evidence that they act as upstream regulators is accumulating, with cotton *GhMAP4K13* positively regulating salt and drought tolerance and rice *OsMAP4K6* enhancing salinity tolerance by phosphorylating OsMKK6 (Zeng et al., 2025; Ren et al., 2026); consistently, *StMAPKKKK1* overexpression enhanced tolerance by

promoting antioxidant defense, proline accumulation and chlorophyll content while reducing oxidative damage (Fig. 8, 9), identifying it as a positive upstream regulator that coordinates multiple physiological pathways. As a conserved serine/threonine kinase, *StMAPKKKK1* is likely to act through phosphorylation-dependent signalling and, in addition to canonical MAPK pathways, may target membrane-associated signalling proteins or transcriptional regulators to coordinate ROS homeostasis, osmotic adjustment and stress-responsive gene expression. Although the downstream targets of *StMAPKKKK1* have yet to be determined, the consistent results from overexpression and RNAi lines indicate that this kinase contributes positively to potato tolerance against salinity and drought stress. Further, phosphoproteomic analysis and protein–protein interaction studies will be required to define its downstream network and molecular targets. Finally, several limitations must be acknowledged: the work was conducted solely under controlled greenhouse conditions using a single cultivar, and functional characterization relied only on overexpression and RNA interference without a complete loss-of-function knockout mutant, so future studies should employ multiple germplasm resources and multi-environment field trials to validate functional stability and agronomic value, and should use CRISPR/Cas9 to generate precise knockout lines for more rigorous validation, thereby refining the mechanistic framework of StMAP4K-mediated abiotic stress responses in potato.

5. Conclusion

In this study, we provide a comprehensive genome-wide identification and characterization of the *StMAPKKKK* gene family in potato, offering new insights into its evolutionary features and potential biological functions. Among the family members, *StMAPKKKK1* was most strongly induced by salinity and drought stress and showed the highest relative transcript levels; the StMAPKKKK1 protein localized to the plasma membrane and cytoplasm. Y2H, BiFC, and SLC assays demonstrated that StMAPKKKK1 physically associates with StMAPKK2, and *StMAPKK2* transcript levels were also elevated under salt stress in *StMAPKKKK1*-overexpressing plants. Phenotypic analyses of *StMAPKKKK1*-OE and RNAi lines indicate that *StMAPKKKK1* positively regulates salt and drought tolerance by promoting plant growth, antioxidant activity, proline accumulation, and chlorophyll retention while reducing H_2O_2 and MDA accumulation.

CRediT authorship contribution statement

X.Z., X.D., and H.S. planned and designed the research. X.D., X.Z., N.Z., Z.H., X.P., Y.Z., D.Z., H.J., Z.C., Y.M., and H.S. collected the data. X.D., X.Z., N.Z., Z.H., X.P., Y.Z., D.Z., H.J., Z.C., Y.M., and H.S. analyzed the data. X.Z., X.D., and H.S. drafted and revised the manuscript. All authors have read and agreed to the published version of the manuscript.

Funding

This Research Program was financially supported by the National Natural Science Foundation of China (Grant No. 32360459), the Natural Science Foundation of Guangdong Province, China (Grant No. 2024A1515010068), and the Hainan Provincial Natural Science Foundation of China (Grant No. 322MS116, 323MS095, 324MS098, 325MS125).

Declaration of competing interests

The authors declare that they have no known competing financial interests or personal relationships that could have appeared to influence the work reported in this paper.

Acknowledgments

We thank Professor Si Huaijun and Professor Zhang Ning from the State Key Laboratory of Aridland Crop Science and the Life Science and Technology, Gansu Agricultural University, for their guidance and assistance in experimental techniques. Additionally, we would like to express our appreciation to Rongkai Wang (Bioediates, Shaanxi, China) for providing the plasmids pBI121-EGFP, pHANNI-BAL, and pART, as well as the construction of overexpression vectors and RNAi expression vectors.

Appendix A. Supplementary data

Supplementary Fig. S1. Multiple sequence alignment of StMAPKKKK proteins from potato and AtMAPKKKK proteins from *Arabidopsis thaliana*. **Fig. S2.** Chromosomal distribution of *StMAPKKKKs* in potato. **Fig. S3**. Sequence logos of the 20 conserved motifs identified in the potato StMAPKKKK protein family. **Fig. S4.** Regional collinearity of *StMAPKKKK* genes in potato. **Fig. S5.** Synteny analysis of *StMAPKKKK* genes between potato and two other plant species (*Arabidopsis thaliana* and *Oryza sativa*). **Fig. S6.** Identification and distribution of cis-regulatory elements in the promoter regions of *StMAPKKKKs* in potato. **Fig. S7.** Tissue-specific expression profiles of eight *StMAPKKKK* genes in potato. **Fig. S8.** Generation and relative expression analysis of *StMAPKKKK1*-OE and RNAi transgenic potato plants. **Fig. S9.** Expression profiles of *StMAPKK2* in *StMAPKKKK1*-transgenic potato lines under salt and drought stress simulations. **Supplementary Table S1.** Sequences of primers used in the present study. **Table S2.** Physicochemical properties of the 8 *MAPKKKK* gene family members in potato. **Table S3.** Information on *MAPKKKKs* in potato, *Arabidopsis thaliana*, and rice. **Table S4.** Ka/Ks analysis of duplicated *StMAPKKKK* gene pairs in potato. **Table S5.** Syntenic relationships of *MAPKKKK* genes from *Solanum tuberosum* (St) with those from *Arabidopsis thaliana* (At), and *Oryza sativa* (Os). **Table S6.** Statistical results of cis-regulatory elements in the promoter region of *StMAPKKKKs* in potato. **Supplementary Data 1:** Analysis of Biochemical and Physiological Indicators.

Data availability

Data will be made available on request.

References

Aebi, H., 1984. “Catalase in Vitro,” in Methods in Enzymology, Ed. L. Packer (San Diego, California: Academic Press) 105, 121–126. https://doi.org/10.1016/s0076-6879(84)05016-3

Bai, J.P., Gao, H.J., Yang, H.Y., Lou, Y., Zhang, J.L., Wang, D., Zhang, J.L., 2016. Comparison of ultrastructural and physiological changes of potato (Solanum tuberosum L.) plantlets subjected to salt and modeling drought stresses. Acta Physiol. Plant. 38(7), 182. https://doi.org/10.1007/s11738-016-2202-y

Bailey, T.L., Johnson, J., Grant, C.E., Noble, W.S., 2015. The MEME suite. Nucleic Acids Res. 43(W1), W39-W49. https://doi.org/10.1093/nar/gkv416

Bates, L.S., Waldren, R.P.A., Teare, I.D., 1973. Rapid determination of free proline for water-stress studies. Plant Soil 39(1), 205-207. https://doi.org/10.1007/BF00018060

Bechtold, U., Field, B., 2018. Molecular mechanisms controlling plant growth during abiotic stress. J Exp. Bot. 69(11), 2753-2758. https://doi.org/10.1093/jxb/ery157

Blum, M., Chang, H.Y., Chuguransky, S., Grego, T., Kandasaamy, S., Mitchell, A., Nuka, G., Paysan-Lafosse, T., Qureshi, M., Raj, S., Richardson, L., 2021. The InterPro protein families and domains database: 20 years on. Nucleic Acids Res. 49(D1), D344-D354. https://doi.org/10.1093/nar/gkaa977

Bravo Iniguez, A., Sun, Q., Du, M., Zhu, M.J., 2026. Unearthing the bioactive properties of potato (*Solanum tuberosum*) for improving metabolic health. Crit. Rev. Food Sci. Nutr. 66(28), 5549–5568. https://doi.org/10.1080/10408398.2026.2662981

Camacho, C., Coulouris, G., Avagyan, V., Ma, N., Papadopoulos, J., Bealer, K., Madden, T.L., 2009. BLAST+: architecture and applications. BMC Bioinform.10(1), 421. https://doi.org/10.1186/1471-2105-10-421

Champion, A., Picaud, A. and Henry, Y., 2004. Reassessing the MAP3K and MAP4K relationships. Trends Plant Sci. 9(3), 123-129. https://doi.org/10.1016/j.tplants.2004.01.005

Chao, J., Li, Z., Sun, Y., Aluko, O.O., Wu, X., Wang, Q., Liu, G., 2021. MG2C: A user-friendly online tool for drawing genetic maps. Mol. Hortic. 1(1), 16. https://doi.org/10.1186/s43897-021-00020-x Chen, H., Zou, Y., Shang, Y., Lin, H., Wang, Y., Cai, R., Tang, X., Zhou, J.M., 2008. Firefly luciferase complementation imaging assay for protein-protein interactions in plants. Plant Physiol. 146(2),368. https://doi.org/10.1104/pp.107.111740

Chen, C., Wu, Y., Li, J., Wang, X., Zeng, Z., Xu, J., Liu, Y., Feng, J., Chen, H., He, Y., Xia, R., 2023. TBtools-II: A "one for all, all for one" bioinformatics platform for biological big-data mining. Mol. Plant, 16(11), 1733-1742. https://doi.org/10.1016/j.molp.2023.09.010 Colcombet, J., Hirt, H., 2008. *Arabidopsis* MAPKs: a complex signalling network involved in multiple biological processes. Biochem. J. 413(2), 217-226. https://doi.org/10.1042/BJ20080625

Dan, I., Watanabe, N.M., Kusumi, A., 2001. The Ste20 group kinases as regulators of MAP kinase cascades. Trends Cell Biol. 11(5), 220-230. https://doi.org/10.1016/S0962-8924(01)01980-8

Edgar, R.C., 2004. MUSCLE: a multiple sequence alignment method with reduced time and space complexity. BMC bioinform. 5(1), 113. https://doi.org/10.1186/1471-2105-5-113

Eddy, S.R., 2011. Accelerated profile HMM searches. PLoS Comput. Biol. *7*(10), e1002195. https://doi.org/10.1371/journal.pcbi.1002195 Fields, S., Song, O.K., 1989. A novel genetic system to detect protein–protein interactions. Nature 340(6230), 245-246. https://doi.org/10.1038/340245a0 Gasteiger, E., Hoogland, C., Gattiker, A., Duvaud, S.E., Wilkins, M.R., Appel, R.D., Bairoch, A., 2005. Protein identification and analysis tools on the ExPASy server. In The proteomics protocols handbook (pp. 571-607). Totowa, NJ: Humana press. https://doi.org/10.1385/1-59259-890-0:571

George, T.S., Taylor, M.A., Dodd, I.C., White, P.J., 2017. Climate change and consequences for potato production: a review of tolerance to emerging abiotic stress. Potato Res. 60(3), 239-268. https://doi.org/10.1007/s11540-018-9366-3

Gietz, R.D., Schiestl, R.H., 2007. Large-scale high-efficiency yeast transformation using the LiAc/SS carrier DNA/PEG method. Nat. protoc. 2(1), 38-41. https://doi.org/10.1038/nprot.2007.15

Giannopolitis, C.N., Ries, S.K., 1977. Superoxide dismutase: I. Occurrence in higher plants. Plant Physiol. 59(2), 309‐314. https://doi.org/10.1104/pp.59.2.309

Goodstein, D.M., Shu, S., Howson, R., Neupane, R., Hayes, R.D., Fazo, J., Mitros, T., Dirks, W., Hellsten, U., Putnam, N., Rokhsar, D.S., 2012. Phytozome: a comparative platform for green plant genomics. Nucleic Acids Res. 40(D1), D1178-D1186. https://doi.org/10.1093/nar/gkr944

He, H., Van Breusegem, F., Mhamdi, A., 2018. Redox-dependent control of nuclear transcription in plants. J. Exp. Bot. 69(14), 3359-3372. https://doi.org/10.1093/jxb/ery130

He, N., Wang, Z., Xiang, B., Chen, H., Zhou, W., Sun, X., Wu, X., de Carvalho Teixeira Yassitepe, J.E., Xiang, Y., Dai, M., 2026. Genome-wide characterization and association analysis of the maize MAP4K gene family identify candidate loci for stress resilience and yield improvement. Mol. Breed. 46(7), 68. https://doi.org/10.1007/s11032-026-01691-4

Heath, R.L., Packer, L., 1968. Photo-oxidation in isolated chloroplasts. I. Kinetics and stoichiometry of fatty acid peroxidation. Arch. Biochem. Biophys. 125, 189-198. https://doi:10.1016/0003-9861(68)90654-1

Hu, B., Jin, J., Guo, A.Y., Zhang, H., Luo, J., Gao, G., 2015. GSDS 2.0: an upgraded gene feature visualization server. Bioinform. 31(8), 1296–7. https://doi.org/10.1093/bioinformatics/btu817

Hu, P., Zheng, L., Chen, L., Zhou, Y., Wang, Y., Huang, T., Zhang, H., Ding, Y., 2026. Phosphorylation of *MAP4K1* and *MAP4K2* by *OST1* is required for drought tolerance. Plant J. 125(3), e70723. https://doi.org/10.1111/tpj.70723

Ichimura, K., Shinozaki, K., Tena, G., Sheen, J., Henry, Y., Champion, A., Kreis, M., Zhang, S., Hirt, H., Wilson, C., Heberle-Bors, E., 2002. Mitogen-activated protein kinase cascades in plants: a new nomenclature. Trends Plant Sci. 7(7), 301-308. https://doi.org/10.1016/S1360-1385(02)02302-6

Jiang, Y., Han, B., Zhang, H., Mariappan, K.G., Bigeard, J., Colcombet, J., Hirt, H., 2019. MAP4K4 associates with BIK1 to regulate plant innate immunity. EMBO Rep. 20(11), EMBR201947965. https://doi.org/10.15252/embr.201947965

Jonak, C., Ökrész, L., Bögre, L., Hirt, H., 2002. Complexity, cross-talk, and integration of plant MAP kinase signalling. Curr. Opin. Plant Biol. 5(5), 415-424. https://doi.org/10.1016/S1369-5266(02)00285-6

Jones, P., Binns, D., Chang, H.Y., Fraser, M., Li, W., McAnulla, C., McWilliam, H., Maslen, J., Mitchell, A., Nuka, G., Pesseat, S., 2014. InterProScan 5: genome-scale protein function classification. Bioinform. 30(9), 1236-1240. https://doi.org/10.1093/bioinformatics/btu031 Jouannic, S., Hamal, A., Leprince, A.S., Tregear, J.W., Kreis, M., Henry, Y., 1999. Characterization of novel plant genes encoding *MEKK/STE11* and RAF-related protein kinases. Gene 229(1-2), 171-181. https://doi.org/10.1016/S0378-1119(99)00012-8

Kaufmann, K., Pajoro, A., Angenent, G.C., 2010. Regulation of transcription in plants: mechanisms controlling developmental switches. Nat. Rev. Genet. 11(12), 830-842. https://doi.org/10.1038/nrg2885

Komis, G., Šamajová, O., Ovečka, M., Šamaj, J., 2018. Cell and developmental biology of plant mitogen-activated protein kinases. Annu. Rev. Plant Biol. 69, 237-265. https://doi.org/10.1146/annurev-arplant-042817-040314

Krzywinski, M., Schein, J., Birol, I., Connors, J., Gascoyne, R., Horsman, D., Jones, S.J., Marra, M.A., 2009. Circos: an information aesthetic for comparative genomics. Genome Res. 19(9), 1639-1645. https://doi.org/10.1101/gr.092759.109

Lamesch, P., Berardini, T.Z., Li, D., Swarbreck, D., Wilks, C., Sasidharan, R., Muller, R., Dreher, K., Alexander, D.L., Garcia-Hernandez, M., Karthikeyan, A.S., 2012. The *Arabidopsis* Information Resource (TAIR): improved gene annotation and new tools. Nucleic Acids Res. 40(D1), D1202-D1210. https://doi.org/10.1093/nar/gkr1090

Lescot, M., Déhais, P., Thijs, G., Marchal, K., Moreau, Y., Van de Peer, Y., Rouzé, P., Rombauts, S., 2002. PlantCARE, a database of plant cis-acting regulatory elements and a portal to tools for in silico analysis of promoter sequences. Nucleic Acids Res. 30(1), 325. https://doi.org/10.1093/nar/30.1.325 Levy, D., Coleman, W.K., Veilleux,

R.E., 2013. Adaptation of potato to water shortage: irrigation management and enhancement of tolerance to drought and salinity. Am. J. Potato Res. 90(2), 186-206. https://doi.org/10.1007/s12230-012-9291-y

Li, G., Cao, C., Yang, H., Wang, J., Wei, W., Zhu, D., Gao, P., Zhao, Y., 2020. Molecular cloning and potential role of DiSOC1s in flowering regulation in *Davidia involucrata Baill*. Plant Physiol. Biochem. 157, 453-459. https://doi:10.1016/j.plaphy.2020.11.003

Li, L., Zhu, T., Wen, L., Zhang, T., Ren, M., 2024a. Biofortification of potato nutrition. J. Adv. Res. 75, 23-34. https://doi.org/10.1016/j.jare.2024.10.033

Li, Y., Li, Y., Zou, X., Jiang, S., Cao, M., Chen, F., Yin, Y., Xiao, W., Liu, S., Guo, X., 2024b. Bioinformatic identification and expression analyses of the MAPK–MAP4K gene family reveal a putative *functional MAP4K10-MAP3K7/8-MAP2K1/11-MAPK3/6* cascade in wheat (*Triticum aestivum* L.). Plants 13(7), 941. https://doi.org/10.3390/plants13070941

Lim, C.W., Baek, W., Cho, J., Lee, S.C., 2025. The pepper MAP4K kinase *CaMAP4K3* negatively regulates drought resistance. Crop J. 13(3), 860-872. https://doi.org/10.1016/j.cj.2025.03.002

Livak, K.J., Schmittgen, T.D., 2001. Analysis of relative gene expression data using real-time quantitative PCR and the $2^{-\Delta\Delta CT}$ method. Methods 25(4), 402-408. https://doi.org/10.1006/meth.2001.1262

Loreto, F., Velikova, V., 2001. Isoprene produced by leaves protects the photosynthetic apparatus against ozone damage, quenches ozone products, and reduces lipid peroxidation of cellular membranes. Plant Physiol. 127(4), S1781-1787. https://doi.org/10.1104/pp.010497

Luker, K.E., Smith, M.C., Luker, G.D., Gammon, S.T., Piwnica-Worms, H., Piwnica-Worms, D., 2004. Kinetics of regulated protein–protein interactions revealed with firefly luciferase complementation imaging in cells and living animals. Proc. Natl. Acad. Sci. 101(33), 12288-12293. https://doi.org/10.1073/pnas.0404041101

Lu, H., Klocko, A.L., Brunner, A.M., Ma, C., Magnuson, A.C., Howe, G.T., An, X., Strauss, S.H., 2019. RNA Interference suppression of AGAMOUS and SEEDSTICK alters floral organ identity and impairs floral organ determinacy, ovule differentiation, and seed hair development in Populus. New Phytol. 222(2), 923–937. https://doi:10.1111/nph.15648

Luo, X., Ye, X., Chen, M., Zhao, D., Li, F., 2025. Comprehensive transcriptome analysis reveals *StMAPK7* regulates cold response in potato. Plant Physiol. Biochem. 223, 109743. https://doi.org/10.1016/j.plaphy.2025.109743

Luo, Y., Wang, K., Zhu, L., Zhang, N., Si, H., 2024. StMAPKK5 Positively Regulates Response to Drought and Salt Stress in Potato. Int. J. Mol. Sci. 25(7), 3662. https://doi.org/10.3390/ijms25073662

Maehly, A.C., Chance, B., 1954. "The assay of catalases and peroxidases," in Methods of biochemical analysis, Ed. D. Glick, (New York, USA: Interscience Publishers) 1, 357–424. https://doi:10.1002/9780470110171.ch14

Majeed, Y., Zhang, N., Zhu, X., Liu, S., Si, H., 2024. *StMAPK10* gene functional identification and analysis in drought resistance of potato crop (*Solanum tuberosum* L.). Physiol. Plant. 176(3), e14362. https://doi.org/10.1111/ppl.14362

Manna, M., Rengasamy, B., Sinha, A.K., 2023. Revisiting the role of the MAPK signaling pathway in plants and its manipulation for crop improvement. Plant, Cell Environ. 46(8), 2277-2295. https://doi.org/10.1111/pce.14606

Mistry, J., Chuguransky, S., Williams, L., Qureshi, M., Salazar, G.A., Sonnhammer, E.L.L., Tosatto, S.C.E., Paladin, L., Raj, S., Richardson, L.J., Finn, R.D., Bateman, A., 2021. Pfam: The protein families' database in 2021. Nucleic Acids Res. 49(D1), D412-D419. https://doi.org/10.1093/nar/gkaa913

Nakano, Y., Asada, K., 1981. Hydrogen peroxide is scavenged by 1156 ascorbate-specific peroxidase in spinach chloroplasts. Plant Cell Physiol. 22, 867–880. https://doi:10.1093/oxfordjournals.pcp.a076232

Nei, M., Gojobori, T., 1986. Simple methods for estimating the numbers of synonymous and nonsynonymous nucleotide substitutions. Mol. Biol. Evol. 3(5), pp.418-426. https://doi.org/10.1093/oxfordjournals.molbev.a040410
Ouyang, S., Zhu, W., Hamilton, J., Lin, H., Campbell, M., Childs, K., Buell, C.R., 2007. The TIGR Rice Genome Annotation Resource: improvements and new features. Nucleic Acids Res. 35(Database), D883ids Reshttps://doi.org/10.1093/nar/gkl976

Pan, L., Fonseca de Lima, C.F., Vu, L.D., De Smet, I., 2021. A comprehensive phylogenetic analysis of the MAP4K family in the green lineage. Front. Plant Sci. 12, 650171. https://doi.org/10.3389/fpls.2021.650171

Pedley, K.F., Martin, G.B., 2005. Role of mitogen-activated protein kinases in plant immunity. Curr. Opin. Plant Biol. 8(5), 541-547. https://doi.org/10.1016/j.pbi.2005.07.006

Pham, G.M., Hamilton, J.P., Wood, J.C., Burke, J.T., Zhao, H., Vaillancourt, B., Ou, S., Jiang, J., Buell, C.R., 2020. Construction of a chromosome-scale long-read reference genome assembly for potato. GigaScience 9(9), giaa100. https://doi.org/10.1093/gigascience/giaa100

Qiu, Z., Duan, H., Xia, L., Li, G., Wen, G., Zhang, F., 2023. Texture Analysis of Steaming and Baking Potato Tuber. J. Nucl. Agric. Sci. 37(5), 981-989. https://doi.org/10.11869/j.issn.1000-8551.2023.05.0981

Ren, N., Yang, X., Ju, H., Fu, D., Shen, T., Ni, L., Jiang, M., 2026. *OsMAP4K6* positively regulates salt tolerance via activating *OsMKK6* in rice. Crop J. 14(3), 735-748. https://doi.org/10.1016/j.cj.2025.12.012

Rodriguez, M.C.S., Petersen, M., Mundy, J., 2010. Mitogen-activated protein kinase signaling in plants. Annu Rev Plant Biol. 61(1), 621-49. https://doi.org/10.1146/annurev-arplant-042809-112252

Schütze, K., Harter, K., Chaban, C., 2009. Bimolecular fluorescence complementation assay to monitor protein–protein interactions in tobacco. Methods Mol. Biol. 479, 389–402. https://doi.org/10.1007/978-1-60327-221-6_26

Saitou, N., Nei, M., 1987. The neighbor-joining method: a new method for reconstructing phylogenetic trees. Mol. Biol. Evol. 4(4), 406-425. https://doi.org/10.1093/oxfordjournals.molbev.a040454 Shang, Y., Luo, X., Zhang, H., Chen, M., Yin, W., Cao, Z., Deng, R., Li, Y., Li, F., 2022. Genome-wide identification and analysis of the MAPK and MAPKK gene families in potato (*Solanum tuberosum* L.). Agronomy 13(1), 93. https://doi.org/10.3390/agronomy13010093

Sparkes, I.A., Runions, J., Kearns, A., Hawes, C., 2006. Rapid, transient expression of fluorescent fusion proteins in tobacco plants and generation of stably transformed plants. Nat. Prot. 1, 2019–2025. https://doi.org/10.1038/nprot.2006.286

Taj, G., Agarwal, P., Grant, M., Kumar, A., 2010. MAPK machinery in plants: recognition and response to different stresses through multiple signal transduction pathways. Plant Signal. Behav. 5(11), 1370-1378. https://doi.org/10.4161/psb.5.11.13020

Takemiya, A., Sugiyama, N., Fujimoto, H., Tsutsumi, T., Yamauchi, S., Hiyama, A., Tada, Y., Christie, J.M., Shimazaki, K.I., 2013. Phosphorylation of BLUS1 kinase by phototropins is a primary step in stomatal opening. Nat. Commun. 4(1), 2094. https://doi.org/10.1038/ncomms3094

Tamura, K., Stecher, G., Kumar, S., 2021. MEGA11: Molecular Evolutionary Genetics Analysis Version 11. Mol. Biol. Evol. 38(7), 3022-3027. https://doi.org/10.1093/molbev/msab120Tang, D., Pei, D., Zhang, M., Hu, X., Lu, M., Li, Z., Wang, Y., Wang, Y., Yang, S., Gong, Z., 2025. Phosphorylation-dependent activation of *MAP4K1/2* by *OST1* mediates ABA-induced stomatal closure in *Arabidopsis.* J. Integr. Plant Biol. 67(11), 2912-2928. https://doi.org/10.1111/jipb.70030 Thompson, J.D., Higgins, D.G., Gibson, T.J., 1994. CLUSTAL W: improving the sensitivity of progressive multiple sequence alignment through sequence weighting, position-specific gap penalties and weight matrix choice. Nucleic Acids Res. 22(22), 4673-4680. https://doi.org/10.1093/nar/22.22.4673

Waadt, R., Seller, C.A., Hsu, P.K., Takahashi, Y., Munemasa, S., Schroeder, J.I., 2022. Plant hormone regulation of abiotic stress responses. Nat. Rev. Mol. Cell Biol. 23(10), 680-694. https://doi.org/10.1038/s41580-022-00479-6

Walter, M., Chaban, C., Schütze, K., Batistic, O., Weckermann, K., Näke, C., Blazevic, D., Grefen, C., Schumacher, K., Oecking, C., Harter, K., 2004. Visualization of protein interactions in living plant cells using bimolecular fluorescence complementation. Plant J. 40(3), 428-438. https://doi.org/10.1111/j.1365-313X.2004.02219.x

Wang, K., Zhang, H., Yang, L., Wei, H., Tang, X., Zhang, N., Si, H., 2025. *StMAPKK1* enhances drought and salt tolerance in potato via ROS scavenging and stomatal closure. Plant Physiol. Biochem. 229, 110383. https://doi.org/10.1016/j.plaphy.2025.110383

Wang, Y., Tang, H., DeBarry, J.D., Tan, X., Li, J., Wang, X., Lee, T.H., Jin, H., Marler, B., Guo, H., Kissinger, J.C., 2012. MCScanX: a toolkit for detection and evolutionary analysis of gene synteny and collinearity. Nucleic Acids Res. 40(7), e49-e49. https://doi.org/10.1093/nar/gkr1293Waterhouse, A.M., Procter, J.B., Martin, D.M., Clamp, M., Barton, G.J., 2009. Jalview Version 2—a multiple sequence alignment editor and analysis workbench. Bioinform. 25(9), 1189-1191. https://doi.org/10.1093/bioinformatics/btp033

Wen, S., Jian, H., Shang, L., Kear, P.J., Zhang, M., Li, Y., Yuan, P., Lyu, D., 2025. Comprehensive transcriptional regulatory networks in potato through chromatin accessibility and transcriptome under drought and salt stresses. Plant J. 121(6), e70081. https://doi.org/10.1111/tpj.70081

Xiong, J., Cui, X., Yuan, X., Yu, X., Sun, J., Gong, Q., 2016. The Hippo/STE20 homolog SIK1 interacts with MOB1 to regulate cell proliferation and cell expansion in *Arabidopsis*. J. Exp. Bot. 67(5), 1461-1475. https://doi.org/10.1093/jxb/erv538

Xu, J., Zhang, S., 2015. Mitogen-activated protein kinase cascades in signaling plant growth and development. Trends Plant Sci. 20(1), 56-64. https://doi.org/10.1016/j.tplants.2014.10.001

Zaheer, K., Akhtar, M.H., 2016. Potato production, usage, and nutrition—a review. Crit. Rev. Food Sci. Nutr. 56(5), 711-721. https://doi.org/10.1080/10408398.2012.724479

Zeng, Q., Peng, F., Wang, J., Wang, S., Lu, X., Bakhsh, A., Li, Y., Qaraevna, B.Z., Ye, W., Yin, Z., 2025. Identification of the MAP4K gene family reveals *GhMAP4K13* regulates drought and salt stress tolerance in cotton. Physiol. Plant. 177(1), e70031. https://doi.org/10.1111/ppl.70031

Zhang, M., Zhang, S., 2022. Mitogen-activated protein kinase cascades in plant signaling. J. Integr. Plant Biol. 64(2), 301-341. https://doi.org/10.1111/jipb.13215

Zhang, M., Chiang, Y.H., Toruño, T.Y., Lee, D., Ma, M., Liang, X., Lal, N.K., Lemos, M., Lu, Y.J., Ma, S., Liu, J., 2018. The MAP4 kinase *SIK1* ensures robust extracellular ROS burst and antibacterial immunity in plants. Cell Host Microbe 24(3), 379-391. https://doi.org/10.1016/j.chom.2018.08.007

Zhang, R., Wang, Y., Wang, X., Jiao, S., Lu, Y., Du, Y., Zhang, W., Kang, Y., Liu, Y., Qin, S., 2025. Differential responses of microstructure, antioxidant defense, and plant hormone signaling regulation in potato (*Solanum tuberosum* L.) under drought, alkaline salt, and combined stresses. Sci. Hortic. 341, 114014. https://doi.org/10.1016/j.scienta.2025.114014

Zhou, Z., Bi, G., Zhou, J.M., 2018. Luciferase complementation assay for protein-protein interactions in plants. Curr. Protoc. Plant Biol. 3(1), 42-50. https://doi.org/10.1002/cppb.20066

Zhu, X., Duan, H., Zhang, G., Jin, H., Xu, C., Chen, S., Zhou, C., Chen, Z., Tang, J., Zhang, Y., 2023. *StMAPK1* functions as a thermos-tolerant gene in regulating heat stress tolerance in potato (Solanum tuberosum). Front. Plant Sci. 14, 1218962. https://doi.org/10.3389/fpls.2023.1218962

Zhu, X., Duan, X., Majeed, Y., Luo, J., Guan, N., Zheng, H., Zou, H., Jin, H., Chen, Z., Zhang, Y., 2025d. Functional analysis of the *StWRKY75* gene in response to heat stress in potato (*Solanum tuberosum* L.). Front. Plant Sci. 16, 1617625. https://doi.org/10.3389/fpls.2025.1617625

Zhu, X., Majeed, Y., Duan, X., Wang, K., Duan, H., Luo, J., Guan, N., Zheng, H., Jin, H., Chen, Z., Li, W., 2025b. Functional analysis of the *StMAPK19* gene in response to salt stress in potato (Solanum tuberosum L.). BMC Plant Biol. 25(1), 1561. https://doi.org/10.1186/s12870-025-07434-5

Zhu, X., Majeed, Y., Wang, K., Duan, X., Guan, N., Luo, J., Zheng, H., Zou, H., Jin, H., Chen, Z., Zhang, Y., 2025c. *StMAPKK1* Enhances Thermotolerance in Potato (Solanum tuberosum L.) by Enhancing Antioxidant Defense and Photosynthetic Efficiency Under Heat Stress. Plants 14(15), 2289. https://doi.org/10.3390/plants14152289

Zhu, X., Majeed, Y., Wang, K., Duan, X., Haotian, L., Junfu, L., Nengkang, G., Haifei, Z., Jin, H., Li, W., Chen, S., 2025a. Functional characterization of StMAPK3 in salt stress tolerance of potato (*Solanum tuberosum* L.) through MAPK-mediated signaling networks. Plant Physiol. Biochem. 229, 110818. https://doi.org/10.1016/j.plaphy.2025.110818

Zhu, X., Wang, K., Duan, X., Pang, X., Du, X., Han, Z., Li, W., Chen, S., Jin, H., Chen, Z., Zhang, Y., 2026. Genome-wide identification of StMAPKKKs and functional characterization of *StMAPKKK44* in regulating salt and drought tolerance in potato (*Solanum tuberosum* L.). J. Plant Physiol. 323, 154799. https://doi.org/10.1016/j.jplph.2026.154799

Zhu, X., Zhang, N., Liu, X., Li, S., Yang, J., Hong, X., Wang, F., Si, H., 2021. Mitogen-activated protein kinase 11 (MAPK11) maintains growth and photosynthesis of potato plant under drought conditions. Plant Cell Rep. 40(3), 491-506. https://doi.org/10.1007/s00299-020-02645-6

Zhu, X., Zhang, N., Liu, X., Wang, S., Li, S., Yang, J., Wang, F., Si, H., 2020. *StMAPK3* controls oxidase activity, photosynthesis, and stomatal aperture under salinity and osmosis stress in potato. Plant Physiol. Biochem. 156, 167-177. https://doi.org/10.1016/j.plaphy.2020.09.012

Zhu, X., Li, W., Zhang, N., Jin, H., Duan, H., Chen, Z., Chen, S., Wang, Q., Tang, J., Zhou, J., Zhang, Y., 2024. *StMAPKK5* responds to heat stress by regulating potato growth, photosynthesis, and antioxidant defenses. Front. Plant Sci. 15, 1392425. https://doi:10.3389/fpls.2024.1392425

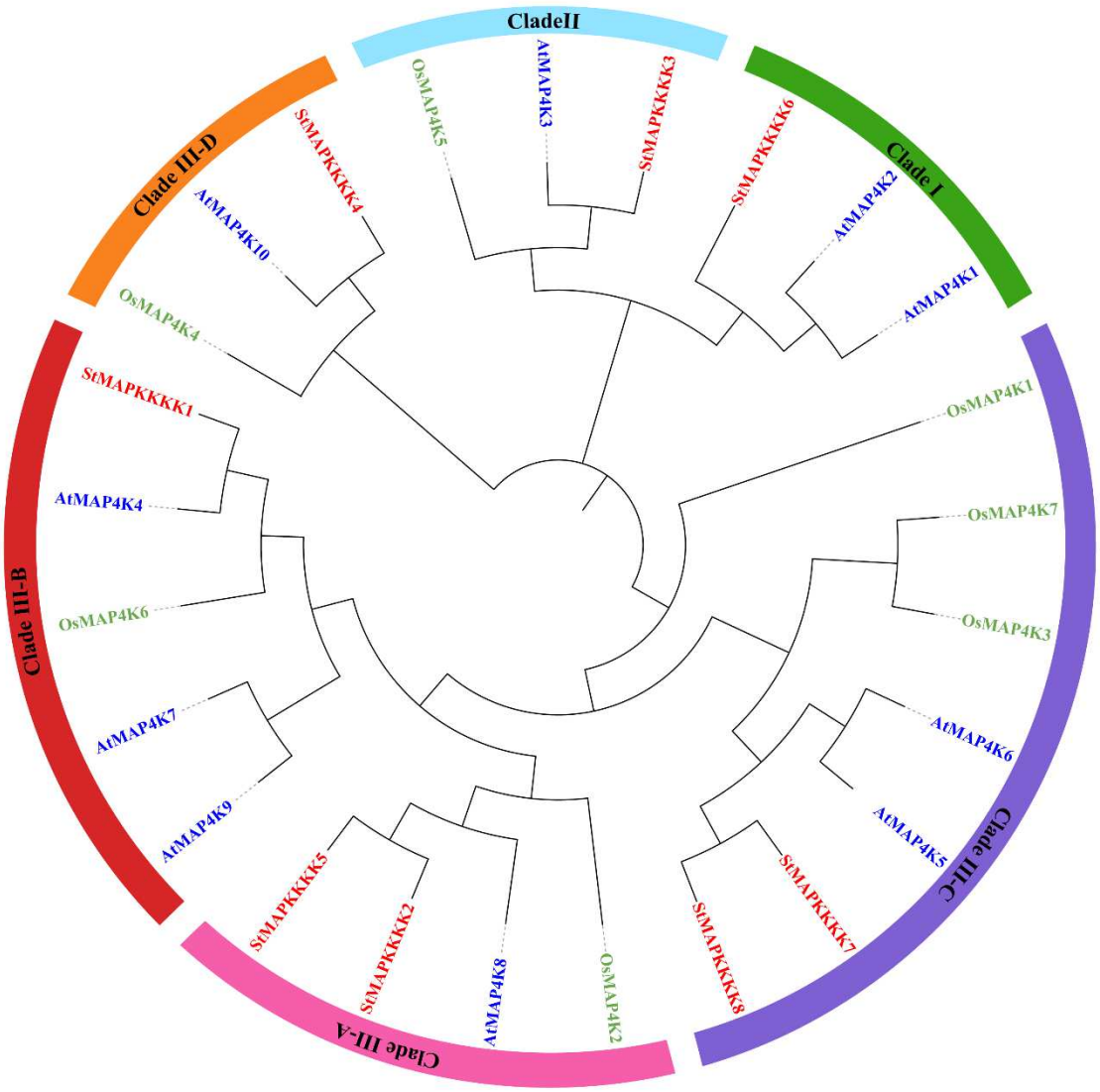


Fig. 1. Phylogenetic tree of MAPKKKK family proteins from potato (*Solanum tuberosum*, St), *Arabidopsis thaliana* (At) and rice (*Oryza sativa*, Os). Amino acid sequences were multi-aligned prior to phylogenetic reconstruction via the Neighbor-Joining (NJ) method with 1000 bootstrap replicates for reliability assessment. All identified MAPKKKK members fell into three primary clades (Clade I, Clade II, Clade III); Clade III was further subdivided into four subclades (III-A, III-B, III-C, III-D), and colored arcs visually mark the boundary of each clade and subclade.

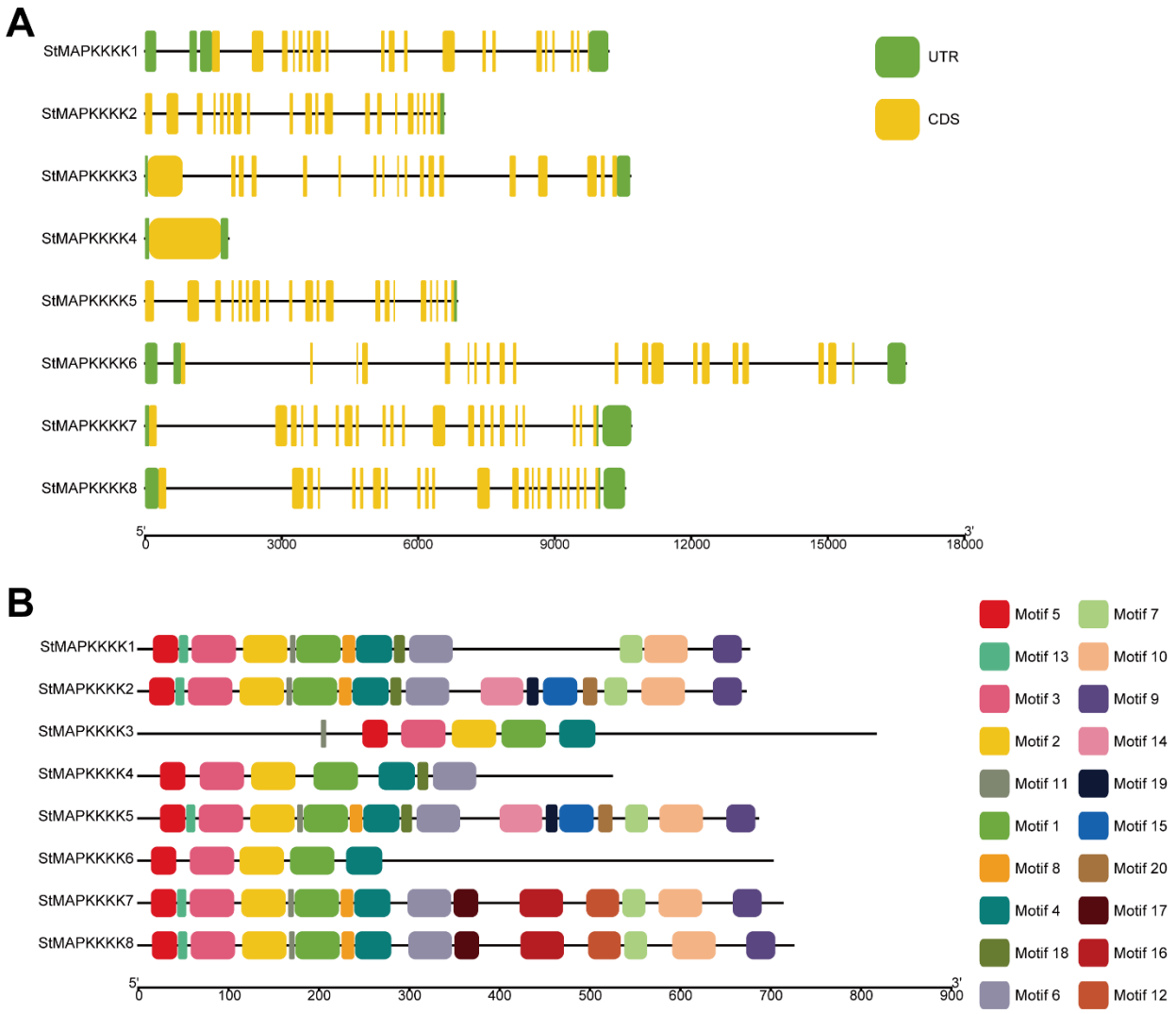


Fig. 2. Analysis of gene structure and conserved protein motifs for eight StMAPKKKK family members in potato. (**A**) Exon–intron and UTR organization at the genomic level. Yellow boxes indicate CDS regions, green boxes indicate UTRs, and black lines represent introns. The x-axis shows genomic coordinate (base pair, bp) along the 5′–3′ direction. (**B**) Distribution of conserved motifs identified via MEME analysis on StMAPKKKK protein sequences. Each colored block matches one numbered motif annotated in the right legend; individual proteins contain 5 to 17 conserved motifs in total. The x-axis denotes amino acid residue positions from the N-terminus to the C-terminus.

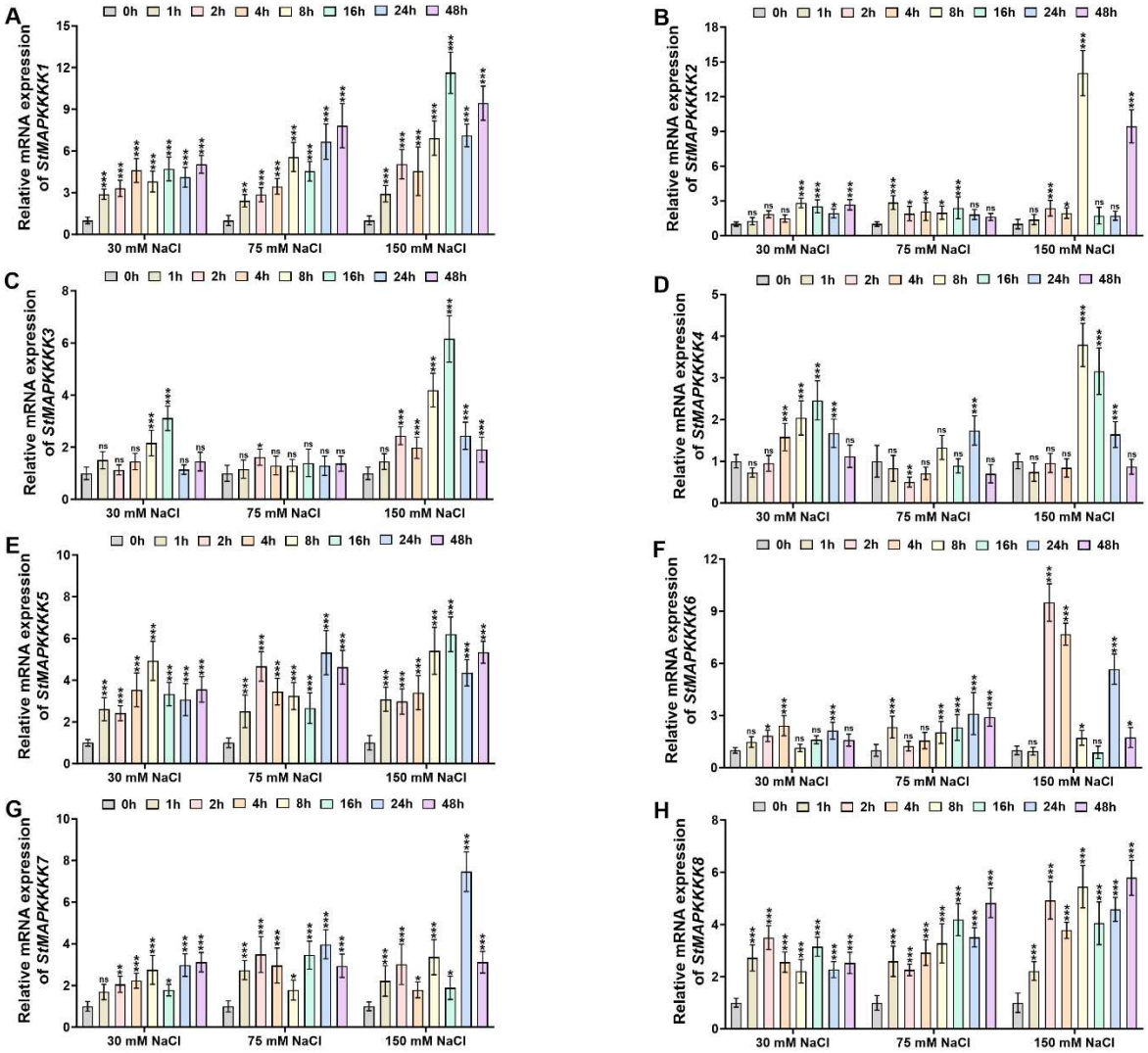


Fig. 3. Expression profiles of eight *StMAPKKKK* family members in potato under salt stress. Relative mRNA abundance of the eight *StMAPKKKK* family members was quantified by qRT-PCR in potato plants treated with 30, 75 or 150 mM NaCl and harvested at 0, 1, 2, 4, 8, 16, 24 and 48 h after treatment. Panels **A**–**H** show *StMAPKKKK1* to *StMAPKKKK8*, respectively. Transcript levels were normalized to *StEF1α* and are expressed relative to the 0 h time point within each NaCl treatment, which was set to 1. Values are the mean ± SD of nine replicates (n = 9). Asterisks denote statistically significant differences relative to the corresponding 0 h control within each NaCl concentration, as determined by two-way ANOVA (NaCl concentration × time) followed by Tukey's multiple comparison test: *$P <$ 0.05, **$P < 0.01$, ***$P < 0.001$; ns, not significant ($P \geq 0.05$).

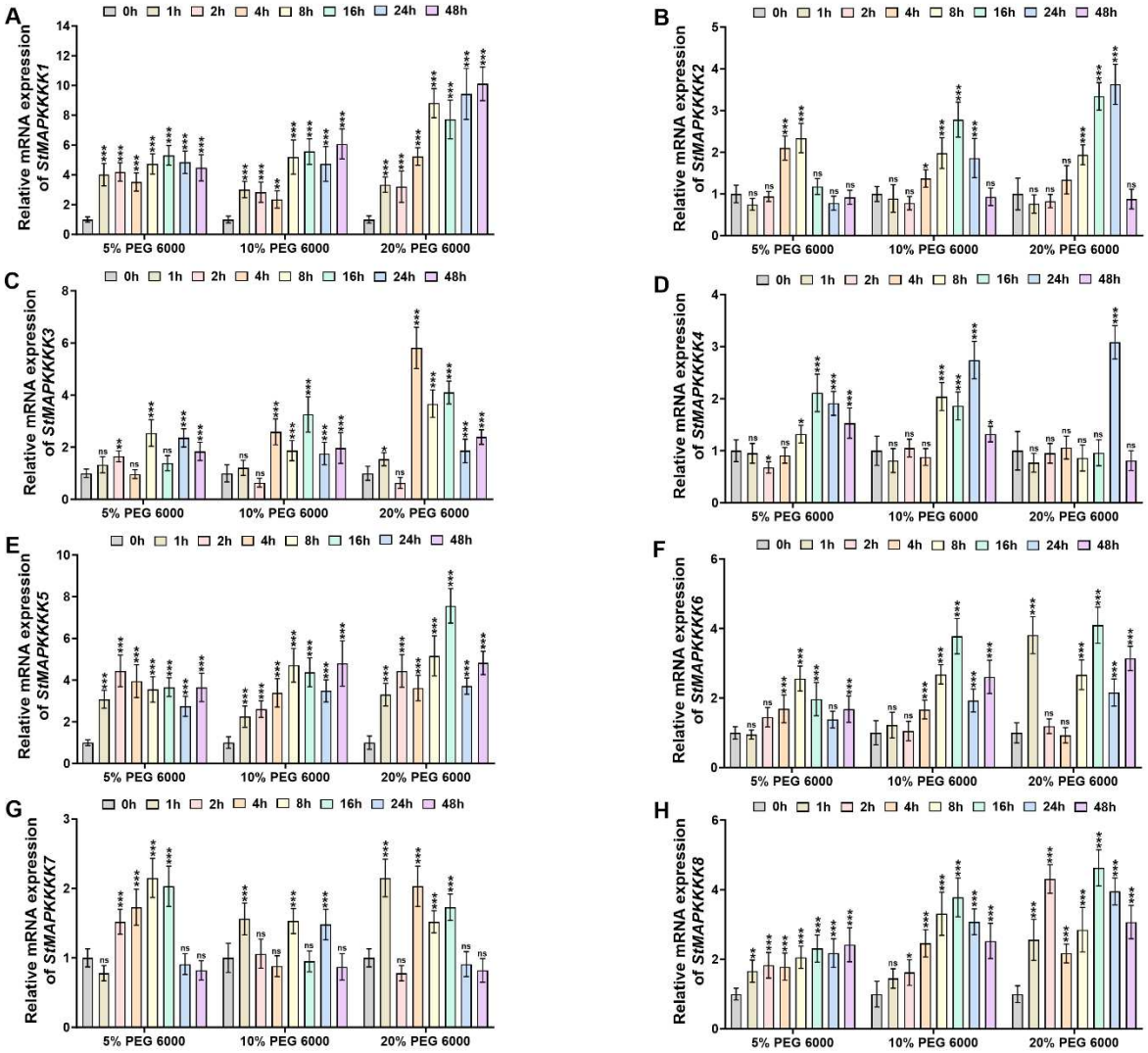


Fig. 4. Expression profiles of eight *StMAPKKKK* family members in potato under drought stress. Relative mRNA abundance of the eight *StMAPKKKK* family members was quantified by qRT-PCR in potato plants treated with 5%, 10% or 20% (w/v) PEG-6000 and harvested at 0, 1, 2, 4, 8, 16, 24 and 48 h after treatment. Panels **A**–**H** show *StMAPKKKK1* to *StMAPKKKK8*, respectively. Transcript levels were normalized to *StEF1α* and are expressed relative to the 0 h time point within each PEG-6000 treatment, which was set to 1. Values are the mean ± SD of nine replicates (n = 9). Asterisks denote statistically significant differences relative to the corresponding 0 h control within each PEG-6000 concentration, as determined by two-way ANOVA (PEG-6000 concentration × time) followed by Tukey's multiple comparison test: *$P < 0.05$, **$P < 0.01$, ***$P < 0.001$; ns, not significant ($P \geq 0.05$).

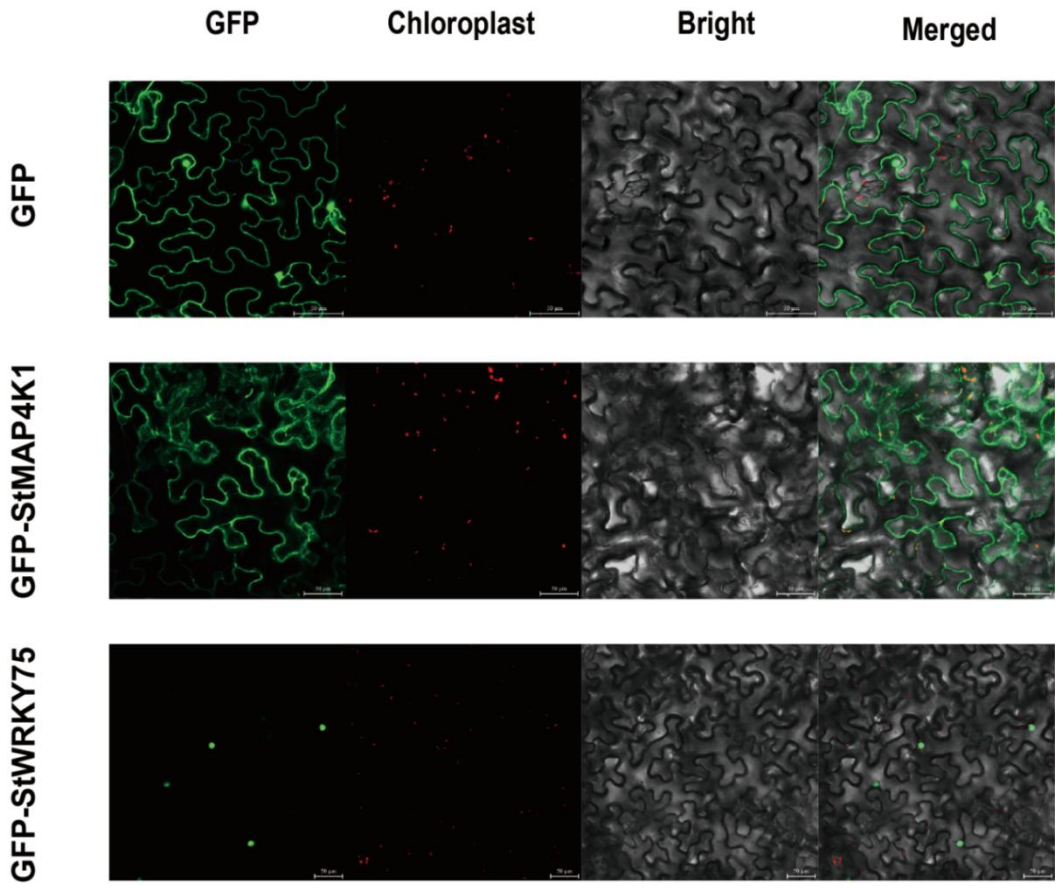


Fig. 5. Subcellular localization of StMAPKKKK1 in *Nicotiana benthamiana* leaf epidermal cells. The pCAM35-GFP empty vector (top row), pCAM35-GFP–StMAPKKKK1 (middle row) and pCAM35-GFP–StWRKY75 (bottom row), the latter serving as a nuclear localization control, were transiently expressed in *N. benthamiana* leaves by *Agrobacterium*-mediated infiltration. For each construct, confocal images were acquired in the GFP channel (green), the chloroplast autofluorescence channel (magenta) and the bright-field channel, and are presented together with the corresponding merged image. Free GFP fluorescence was distributed throughout the plasma membrane, cytoplasm and nucleus; GFP–StMAPKKKK1 fluorescence localized predominantly to the plasma membrane and cytoplasm; GFP–StWRKY75 fluorescence was restricted to the nucleus. Scale bars = 50 μm (all panels).

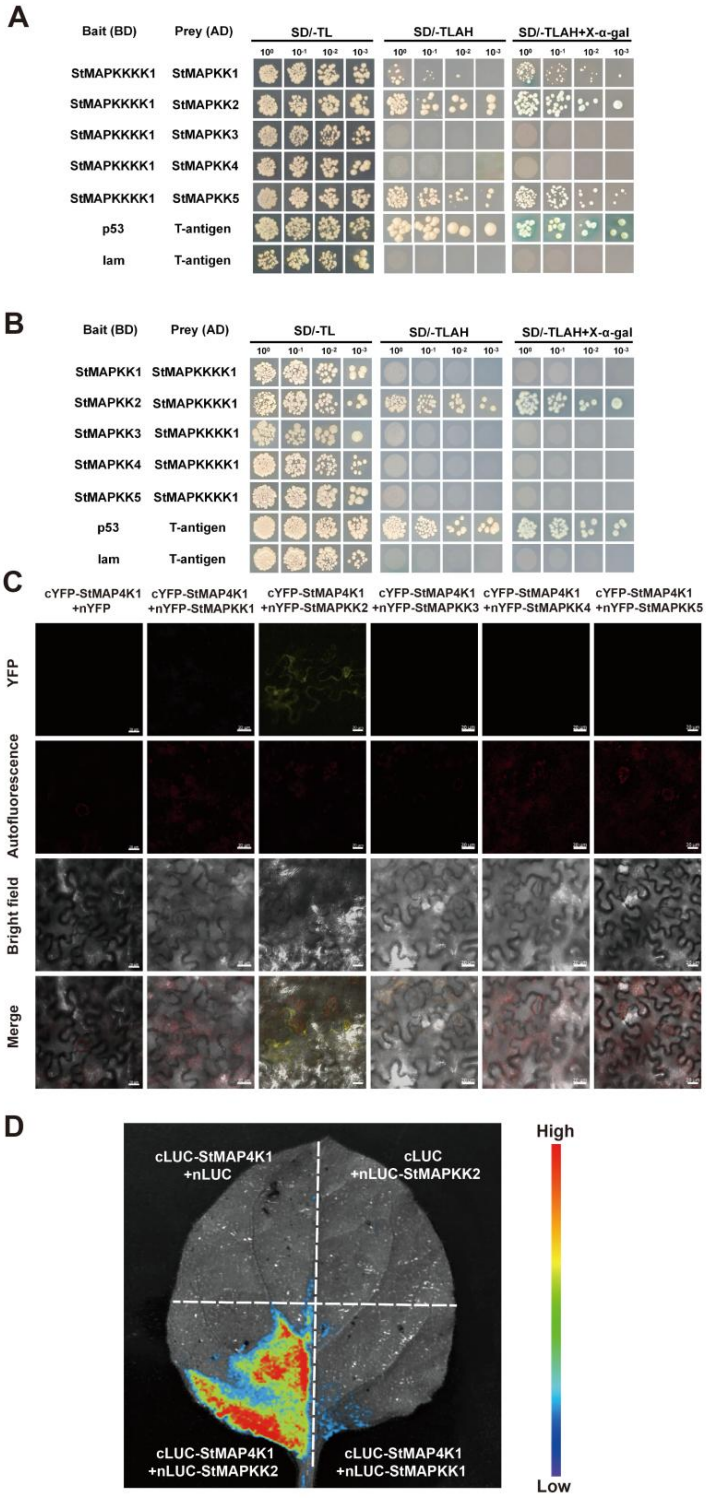


Fig. 6. Validation of protein‑protein interactions between StMAP4K1 (StMAPKKKK1) and StMAPKK family members. (**A**) Yeast two-hybrid (Y2H) assay showing interactions between BD-StMAP4K1 and AD-StMAPKK1-5. Yeast co-transformants were serially diluted (10^0 to 10^{-3}) and spotted onto SD/-TL, SD/-TLAH, and SD/-TLAH + X-α-Gal plates. p53/T-antigen and Lam/T-antigen served as the positive and negative controls, respectively. (**B**)

Reciprocal Y2H assay in which BD-StMAPKK1-5 were each paired with AD-StMAP4K1; growth was assessed on the same selective media as in (**A**). (**C**) BiFC assay showing the interaction of StMAP4K1 with StMAPKK2 in *Nicotiana benthamiana* leaf epidermal cells. cYFP-StMAP4K1 was co-expressed with nYFP-StMAPKK1-5, and YFP fluorescence was detected only in the combination with StMAPKK2. YFP, chloroplast autofluorescence (Auto), bright-field, and merged images are shown. Scale bars = 20 μ m. (**D**) Split-luciferase complementation (SLC) assay confirming the StMAP4K1-StMAPKK2 interaction in *N. benthamiana* leaves. cLUC-StMAP4K1 + nLUC-StMAPKK2 was the experimental combination, whereas cLUC + nLUC, cLUC + nLUC-StMAPKK2, cLUC-StMAP4K1 + nLUC, and cLUC-StMAP4K1 + nLUC-StMAPKK1 served as negative controls. The color scale indicates luminescence intensity from low to high.

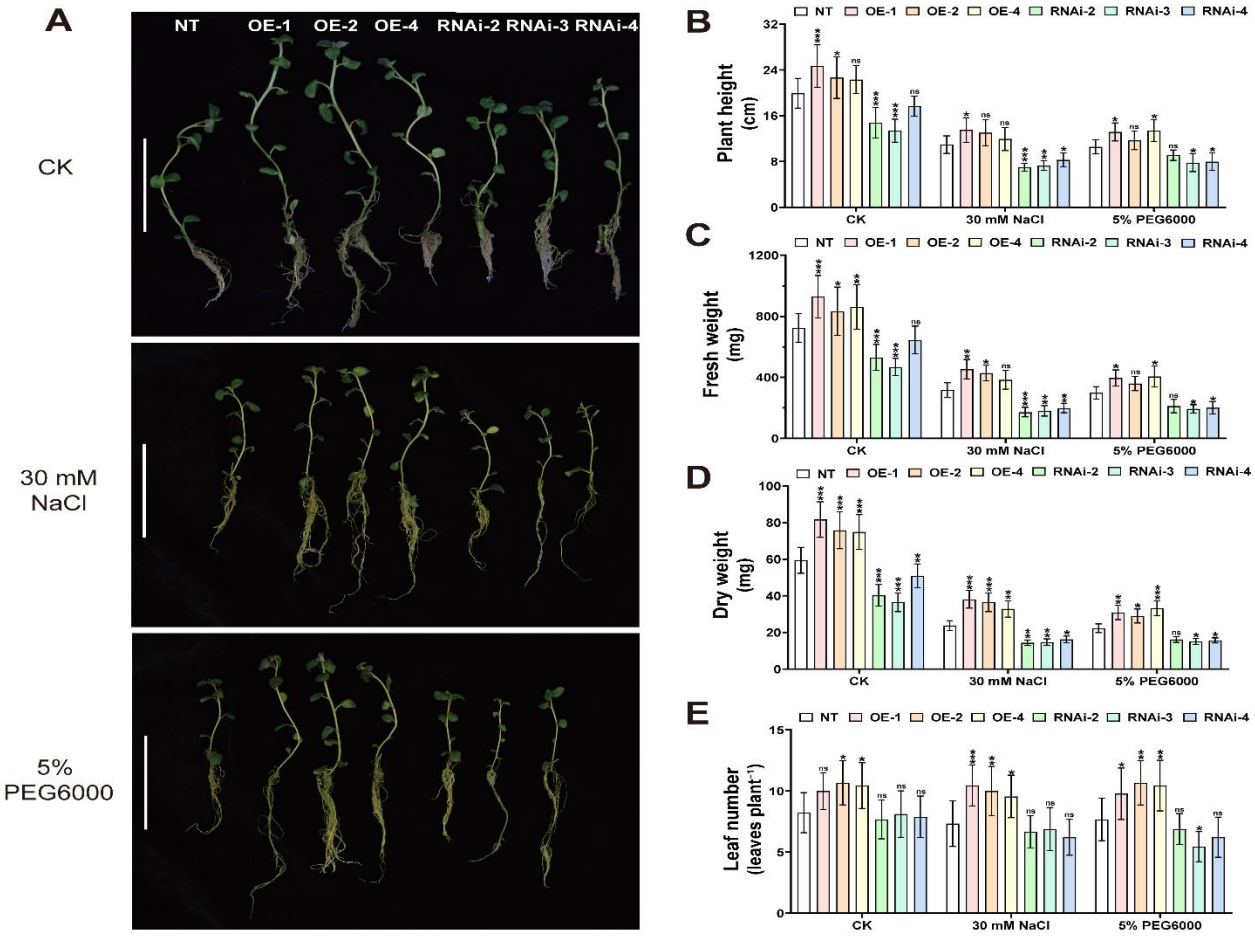


Fig. 7. Growth phenotypes and agronomic traits of NT, *StMAPKKK1*-OE and *StMAPKKK1*-RNAi potato lines under control, salt and PEG-6000-simulated drought stress. (**A**) Representative whole-plant morphology of NT, *StMAPKKK1*-OE (OE-1, OE-2, OE-4) and *StMAPKKK1*-RNAi (RNAi-2, RNAi-3, RNAi-4) lines grown under control (CK), 30 mM NaCl or 5% (w/v) PEG-6000 conditions. Scale bar = 10 cm (applies to all panels). (**B**–**E**) Quantification of plant height (**B**), fresh weight (**C**), dry weight (**D**) and leaf number per plant (**E**) under the three treatments. Values are the mean ± SD of nine plants per genotype per treatment (n = 9). Asterisks denote statistically significant differences relative to the NT control within each treatment, as determined by two-way ANOVA (genotype × treatment) followed by Tukey's multiple comparison test: *$P < 0.05$, **$P < 0.01$, ***$P < 0.001$; ns, not significant ($P \geq 0.05$).

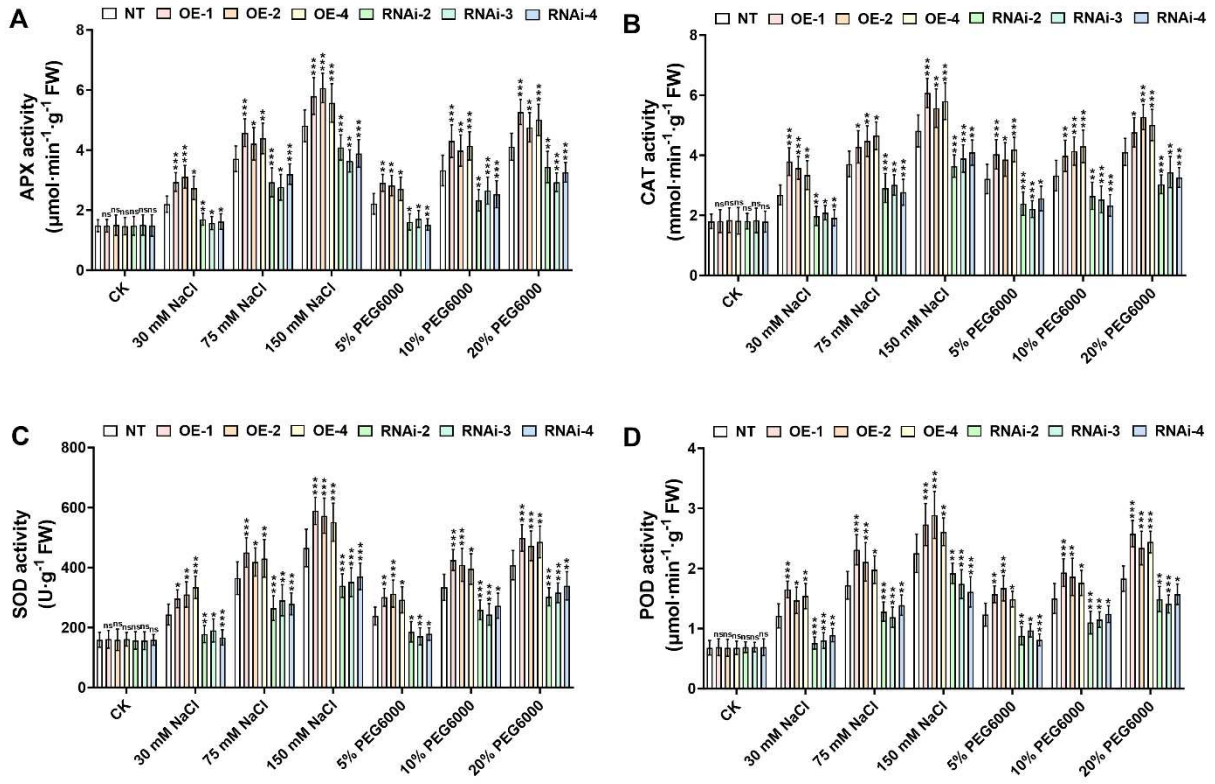


Fig. 8. Antioxidant enzyme activities in NT, *StMAPKKKK1*-OE and *StMAPKKKK1*-RNAi potato lines under salt and PEG-6000-simulated drought stress. (**A**–**D**) Activities of APX (**A**), CAT (**B**), SOD (**C**) and POD (**D**) in NT, *StMAPKKKK1*-OE (OE-1, OE-2, OE-4) and *StMAPKKKK1*-RNAi (RNAi-2, RNAi-3, RNAi-4) lines under control (CK), NaCl (30, 75 and 150 mM) or PEG-6000 (5%, 10% and 20%, w/v) treatment. Enzyme activities are expressed on a fresh weight (FW) basis. Values are the mean ± SD of nine plants per genotype per treatment (n = 9). Asterisks denote statistically significant differences relative to the NT control within each treatment, as determined by two-way ANOVA (genotype × treatment) followed by Tukey's multiple comparison test: $*P < 0.05$, $**P < 0.01$, $***P < 0.001$; ns, not significant ($P \geq 0.05$).

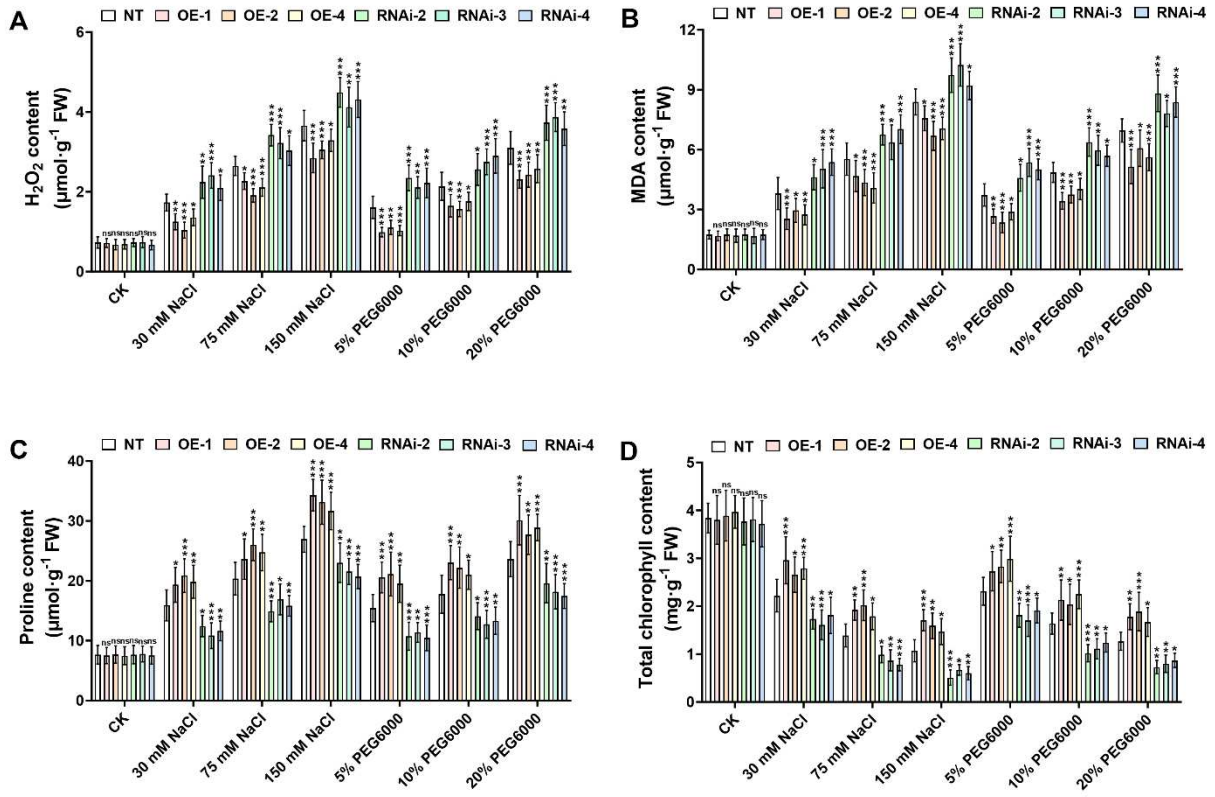


Fig. 9. Physiological parameters in NT, *StMAPKKKK1*-OE and *StMAPKKKK1*-RNAi potato lines under salt and PEG-6000-simulated drought stress. (**A**–**D**) Contents of H_2O_2 (**A**), MDA (**B**), proline (**C**) and total chlorophyll (**D**) in NT, *StMAPKKKK1*-OE (OE-1, OE-2, OE-4) and *StMAPKKKK1*-RNAi (RNAi-2, RNAi-3, RNAi-4) plants under control (CK), NaCl (30, 75 and 150 mM) or PEG-6000 (5%, 10% and 20%, w/v) treatment. Values are expressed on a fresh weight (FW) basis. Values are the mean ± SD of nine plants per genotype per treatment (n = 9). Asterisks denote statistically significant differences relative to the NT control within each treatment, as determined by two-way ANOVA (genotype × treatment) followed by Tukey's multiple comparison test: $*P < 0.05$, $**P < 0.01$, $***P < 0.001$; ns, not significant ($P \geq 0.05$).

Supplementary Files

This is a list of supplementary files associated with this preprint. Click to download.

- SupplementarymaterialsStMAPKKKK120261024.docx
- TableS1Sequencesofprimersusedinthepresentstudy20260708.xlsx
- TableS2IdentificationandbasicinformationofStMAPKKKKgenesinpotato.xlsx
- TableS3InformationonMAPKKKKsinpotatoArabidopsisthalianaandrice.xlsx
- TableS4KaKsanalysisofduplicatedStMAPKKKKgenepairsinpotato.xlsx
- TableS5.ComparativeanalysisofsyntenicgenepairsamongSolanumtuberosumArabidopsisthalianaandOryzasativa.xlsx
- TableS6StatisticalresultsofcisregulatoryelementsinthepromoterregionofStMAPKKKKsinpotato.xlsx
- Fig.S1MultiplesequencealignmentofStMAPKKKKproteinsfrompotatoandAtMAPKKKKproteinsfromArabidopsisthaliana.tif
- Fig.S2ChromosomaldistributionofStMAPKKKKsinpotato.tif
- Fig.S3Sequencelogosofthe20conservedmotifsidentifiedinthepotatoStMAPKKKKproteinfamily.tif
- Fig.S4RegionalCollinearityofStMAPKKKKGenesinPotato.tif
- Fig.S5SyntenyanalysisofStMAPKKKKgenesbetweenpotatoandtwootherplantspecies.jpg
- Fig.S6AnalysisofcisactingelementsintheupstreamregionsofStMAPKKKKs.tif
- Fig.S7ExpressionanalysisofStMAP4Kgenesindifferentorgansfrompotato2.tif
- Fig.S8DetectionofStMAPKKKK1OEandRNAitransgenicpotatoplantsbyRTPCRandqRTPCR..tif